Title

An expanded palette of dopamine sensors for multiplex imaging in vivo.

Authors

Patriarchi, Tommaso
Mohebi, Ali
Sun, Junqing
et al.

Peer reviewed

An expanded palette of dopamine sensors for multiplex imaging *in vivo*

Tommaso Patriarchi[1,6,7,#], **Ali Mohebi**[2,#], **Junqing Sun**[1,4,8,#], **Aaron Marley**[3], **Ruqiang Liang**[1], **Chunyang Dong**[1], **Kyle Pugher**[4], **Grace Or Mizuno**[1], **Carolyn M Davis**[1], **Brian Wiltgen**[4], **Mark von Zastrow**[3,5,*], **Joshua D. Berke**[2,5,*], **Lin Tian**[1,*]

[1]Department of Biochemistry and Molecular Medicine, University of California Davis, Sacramento, CA 95817, USA [2]Department of Neurology, University of California San Francisco, CA 94158, USA [3]Department of Psychiatry, University of California San Francisco, CA 94158, USA [4]Center for Neuroscience, University of California Davis, CA 95616, USA [5]Weill Institute for Neurosciences and Kavli Center for Fundamental Neuroscience, University of California San Francisco, CA [6]Present address: Institute of Pharmacology and Toxicology, University of Zurich, Zurich, Switzerland [7]Neuroscience Center Zurich, University and ETH Zurich, Zurich, Switzerland [8]Key Laboratory of Medical Electrophysiology, Ministry of Education & Medical Electrophysiological Key Laboratory of Sichuan Province, Institute of Cardiovascular Research, Southwest Medical University, Luzhou, China

Abstract

Genetically encoded dopamine sensors based on green fluorescent protein (GFP) enable high-resolution imaging of dopamine dynamics in behaving animals. However, these GFP-based variants cannot be readily combined with commonly used optical sensors and actuators, due to spectral overlap. We therefore engineered red-shifted variants of dopamine sensors called RdLight1, based on mApple. RdLight1 can be combined with GFP-based sensors with minimal

interference, and shows high photostability permitting prolonged continuous imaging. We demonstrate the utility of RdLight1 for receptor-specific pharmacological analysis in cell culture, simultaneous assessment of dopamine release and cell type-specific neuronal activity, and simultaneous subsecond monitoring of multiple neurotransmitters in freely behaving rats. Dual-color photometry revealed that dopamine release in the nucleus accumbens evoked by reward-predictive cues is accompanied by a rapid suppression of glutamate release. By enabling multiplexed imaging of dopamine with other circuit components *in vivo*, RdLight1 opens avenues for understanding many aspects of dopamine biology.

Editorial Summary:

Red and yellow versions of the genetically encoded dopamine sensor dLight1 have been developed and allow multiplexed imaging of dopamine with neurotransmitter or cell-type specific calcium combined with green sensors or actuators as demonstrated ex vivo and in behaving rodents.

Introduction

A recent advance in the measurement of neuromodulators was the development of optical sensors such as dLight1 and GRAB$_{DA}$, intensity-based, genetically encoded indicators for dopamine (DA) with high molecular specificity [1,2]. These sensors bridge the temporal scales of microdialysis and voltammetry by permitting prolonged detection of behaviorally relevant DA fluctuations with high spatial and temporal resolution. Dissemination of e.g. dLight1 has already facilitated discoveries about behavioral conditions and neural mechanisms controlling DA release [4].

Our understanding of how neuromodulators are regulated, and how they influence neural circuits, could be enhanced by combining these sensors with optical measurements of other circuit components. Multiplexed imaging became possible with the introduction of red-shifted genetically encoded calcium indicators [5], which have been increasingly optimized for improved sensitivity and brightness [6]. Non-genetically encoded red-shifted probes for DA imaging based on single-walled carbon nanotubes have been developed, yet their application is currently limited to cultured cells or brain slices [7,8].

Here, we expand the color spectrum of dLight1 to introduce both yellow (YdLight1.1) and red (RdLight1) sensor variants. In HEK293 cells, we establish an *in vitro* assay for optical dissection of drug efficacy at two distinct DA receptor subtypes using RdLight1 and dLight1.5. In striatal slices, we characterize the sensitivity and kinetics of RdLight1 in response to endogenous DA release triggered by electrical stimuli. Finally, we demonstrate multi-color photometry through a single optic fiber in the nucleus accumbens (NAc) of awake behaving rats, compare DA release to postsynaptic neuronal activity in cells with DA D1 receptors, and compare DA and glutamate dynamics in response to reward-predictive cues (Extended Data Fig. 1).

Results

Sensor engineering

To obtain a yellow-shifted DA sensor, named YdLight1, we introduced two point mutations in dLight1.3b (V284Y/S397A, corresponding to V203Y/S72A mutations in EGFP) that were previously shown to yellow-shift the excitation and emission properties of EGFP [9–11] (Fig. 1a, Extended Data Fig. 2a). When expressed in HEK cells, YdLight1 showed a ~12 nm right-shift in the emission peak (525 nm) compared to its parent sensor (Fig. 1b), while maintaining membrane expression and a strong positive response to bath-applied DA (ΔF/F = 306 ± 14 %; Fig. 1 c, d). To generate a red DA sensor, we replaced cpGFP in dLight1.3b with cpmApple and its flanking linker sequences, derived from jRGECO1a (Fig. 1a) [6]. Though it expressed well on the membrane, the initial variant (LSSPV-cpmApple-DQDDL) showed no response to DA (Extended Data Fig. 2b). To improve DA sensitivity, we generated a linker library flanking both sides of cpmApple. Of a total of 264 variants screened, we identified a variant with a strong positive fluorescence response to bath-applied DA (Extended Data Fig. 2c). We then mutated residue Phe[129], which we previously discovered as a site capable of tuning the fluorescence responses of dLight1 [1], to a selected set of amino acids. The F129E variant showed excellent membrane expression and fluorescence response (ΔF/F = 248 ± 7 %) and we thus named this variant RdLight1 (Extended Data Fig. 2d). The emission spectrum measured in HEK293 cells expressing RdLight1 peaks at ~588 nm, with minimal overlap with dLight1.3b (Fig. 1b). When tested for photoactivation upon blue light illumination [6] in HEK293 cells, continuous or burst illumination at 488 nm elicited a negligible increase of fluorescence intensity compared to DA-induced fluorescence changes (Extended Data Fig. 3).

Intrinsic properties of RdLight1.

In situ titrations of DA onto YdLight1- and RdLight1-expressing HEK cells or dissociated hippocampal neurons revealed apparent affinities of the sensors in the physiological range (Fig. 1c,d). RdLight1 is ~350 and ~60 times more sensitive to DA than to norepinephrine (NE) in neurons and HEK293 cells; the maximal response of RdLight1 to NE at 100uM and above was substantially lower compared to DA (Extended Data Fig. 4a,b). We observed negligible responses to all other neurotransmitters tested (acetylcholine, glutamate, serotonin, histamine), except for epinephrine at high concentrations (≥ 10 μM) (Extended Data Fig. 4c). RdLight1 is effectively inert with respect to engagement of endogenous G protein- or b beta-arrestin-mediated signaling mechanisms. In HEK293 cells expressing wild-type D1 receptors, application of the D1 agonist SKF81297 markedly increased cAMP production, indicative of receptor signaling by coupling to stimulatory G proteins (Extended Data Fig. 5a). In contrast, in cells expressing RdLight1, D1 agonist produced no increase above the baseline level observed in GFP-expressing negative control cells (Extended Data Fig. 5a). RdLight1 also does not block G protein signaling because it had no detectable effect on the cAMP response measured in U2OS cells that express D1 endogenously [1] (Extended Data Fig. 5b), nor did it produce any detectable effect on the cAMP response mediated by endogenous D1 in cultured striatal neurons, which express endogenous D1 in ~50% of cells [12] (Extended Data Fig. 5c). We next confirmed that RdLight1 does not engage beta-arrestins. Using live-cell TIRF microscopy to measure agonist-induced receptor

internalization, an indicator of receptor binding to endogenous beta-arrestins[13], Flag-tagged RdLight1 remained in the plasma membrane while Flag-tagged D1 rapidly internalized (Extended Data Fig. 5d,e). We independently verified lack of beta-arrestin engagement with RdLight1 by measuring surface recruitment of GFP-tagged beta-arrestin-2, which is a highly sensitive assay capable of detecting even weak or transient GPCR interactions with beta-arrestin [13]. Whereas D1 robustly mediated agonist-dependent recruitment of beta-arrestin into puncta at the plasma membrane, RdLight1 did not (Extended Data Fig. 5f–i).

Dual-color imaging in cells.

A major advantage enabled by red-shifted probes is their combination with GFP-based reporters in multiplexed imaging experiments [5]. We leveraged this to distinguish spectrally distinct probes pharmacologically. As the GFP-based dLight1.5 is a DRD2-based DA sensor, and is spectrally distinct from the D1-based RdLight1 (Extended Data Fig. 6a), we examined the feasibility to simultaneously monitor responses to subtype-selective drugs. We combined two populations of HEK cells expressing dLight1.5 or RdLight1, respectively, followed by dual-color confocal imaging. Bath application of a selective D2 agonist (quinpirole) led to a green fluorescence increase of dLight1.5 but failed to elicit any response of RdLight1 (Fig 1e,f). Subsequent application of a selective D1 agonist (A77636) led to fluorescence increase of RdLight1 but not of dLight1.5. In fact, A77636 slightly decreased dLight1.5 fluorescence in the combined presence of quinpirole (Fig 1e,f), an observation consistent with A77636 having weak partial agonist activity at D2 receptors [14]. Concentration-response curves of each individual agonist emphasized the high degree of pharmacological selectivity that can be achieved using this multiplex detection strategy (Extended Data Fig. 6b,c). Furthermore, application of subtype-selective antagonists brought the green (Sulpiride) or red (SCH-23390) fluorescence from the peak to the baseline selectively reversed the fluorescence increase in each channel (Fig 1e,f, Supplementary Movie 1).

As RdLight1 selectively responds to DA in neurons, we next tested whether combining RdLight1 with a b_2-adrenergic receptor (b_2AR)-based NE sensor (nLight1.3) [15] would allow optically dissecting these two catecholamines from each other with high molecular specificity. We used a neuron-astrocyte co-culture system to selectively infect neurons and astrocytes with RdLight1 (AAV9-*hSynapsin1*-RdLight1) and nLight1.3 (AAV1-*GFAP*-nLight1.3), respectively, using tissue-specific promoters to maximize expression of both sensors (Fig. 1g). We chose to separate expression of the sensors in different cell populations to avoid possible interference or interaction between sensors (Extended Data Fig. 6d–f). We then performed time-lapse, dual-color imaging during sequential bath application of 1 μM DA, 1 μM NE, the D1-antagonist SCH-23390 (for RdLight1), and the b_2AR antagonist ICI-118551 (for nLight1.3). We observed cell type-specific responses to application of each catecholamine, and reversal by receptor-specific antagonists (Fig. 1h, Supplementary Movie 2).

Simultaneous imaging of DA and glutamate or intracellular calcium transients *ex vivo*

We next examined the sensitivity of RdLight1 to endogenous DA release using two-photon (2P) imaging in striatal slices (Fig. 2a). We infected the dorsal striatum of young mice (8–12 weeks old) with AAV9-*hSynapsin1*-RdLight1 and allowed 2–4 weeks for expression before

acute slice preparation. Upon application of a brief electrical stimulus (0.5 ms), frame scans at high frequency (198 Hz) revealed a rapid fluorescent response with kinetics similar to those previously described for dLight1 (Fig. 2b). RdLight1 robustly reported DA release triggered by electrical stimuli, which we repeated over the course of continuous two-photon imaging, though the baseline fluorescence declined about 17% at the end of the imaging session (Extended Data Fig 7). When we applied a selective DA reuptake blocker (1 μM GBR-12909) to the slice, the decay time of the electrically evoked DA transient was significantly increased (*P=0.009, paired t-test (two-sided)), whereas application of a D1-selective antagonist (10 μM SKF-83566) completely blocked the response (Fig. 2c and d).

A palette of neurotransmitter sensors offers the potential for monitoring multiple transmitters simultaneously at the same location. As the striatum receives both dopaminergic and glutamatergic inputs, we next tested whether we could separately image evoked DA and glutamate transients. We co-injected RdLight1 with the glutamate sensor iGluSnFR [16] (AAV5-*hSynapsin1*-iGluSnFR). We observed a diffuse expression pattern in both green and red channels, which is consistent with the expression pattern of membrane-localized sensors [1,16,17] (Fig. 2e). In response to a single pulse of electrical stimulation, two-photon frame scans revealed fluorescence changes in both green and red channels, with distinct peak amplitudes and decay kinetics (Fig 2f). To further confirm molecular specificity, we applied the excitatory amino acid transporter-2 (EAAT-2) selective blocker (WAY213613, 20 μM), which selectively increased the decay time of the iGluSnFR response (*P=0.005, paired t-test (two-sided)), but not its peak amplitude (P=0.798, paried t-test (two-sided)) (Fig 2f,g). We did not observe significant changes in either the decay time (P=0.123 paired t-test (two-sided)), or the amplitude (P=0.093, paired t-test (two-sided)) of the simultaneously recorded response of RdLight1 with the addition of WAY213613 (Fig. 2f,g, P>0.05).

As a final *ex vivo* experiment we tested whether multiplexed imaging can simultaneously visualize both local DA transients and neuronal activity. We co-injected RdLight1 with GCaMP6s [18] (AAV1-*hSynapsin1*-GCaMP6s) in the striatum. Two to three weeks later, the expression pattern of each sensor could be distinguished by two-photon imaging: GCaMP6s labelled neuronal somata whereas RdLight1 outlined the membrane (Fig. 2h). A train of 20 pulses applied at 40Hz triggered responses from both indicators, and the decay kinetics of calcium transients and DA release were clearly distinct (*P=0.0002 paired t-test (two-sided)) (Fig. 2i,j). Therefore, multiplexed imaging of neurotransmitters and cell type-specific neural activity can be achieved by combining RdLight1 with other GFP-based sensors.

Multiplex measurements of dopamine release with cell-type specific input and output activity *in vivo*

To assess the utility of RdLight1 *in vivo,* we first examined the response of RdLight1 to DA changes in the nucleus accumbens (NAc) triggered by optical stimulation of midbrain DA neurons in freely behaving rats. In TH-Cre rats [19] we infected the ventral tegmental area (VTA) with AAV-*EF1a*-FLEX-ChR2-EYFP [4,20] and the NAc with AAV9-*CAG*-RdLight1 (Fig. 3a, Extended Data Fig 8). Using chronically-implanted optical fibers, we monitored the RdLight1 photometry signal in NAc while delivering laser pulses in VTA to evoke dopamine release (Fig. 3b) [21]. RdLight1 showed clear, frequency-dependent DA increases in response

to optical stimulation, with individual peaks of pulse-evoked DA transients visible at up to 8 Hz (Fig. 3b).

We next performed simultaneous measurements of presynaptic activity in DA terminals (using GCaMP6f) and the resulting DA release. In TH-Cre rats we infected VTA with Cre-dependent, axon-targeted GCaMP6f (AAV1-*hSynapsin1*-FLEX-axonGCaMP6f; [22]) and NAc with RdLight1 (AAV9-CAG-RdLight1), then recorded dual-color photometry signals through a single optic fiber in NAc (Fig.3c–g Extended Data Fig 8). Rats were freely moving within an operant chamber, and uncued sugar pellet rewards were delivered at random intervals (with an audible click of the food hopper). RdLight1 displayed minimal photobleaching over the long duration of these experiments (Fig. 3c) with consistent signal changes to unpredicted rewards. Reward delivery evoked rapid increases in both GCaMP6f and RdLight1 signals, with a similar time course (Fig. 3d, e). The session-wide cross-correlation between presynaptic calcium and DA release was strong (peak cross-correlation = 0.86) (Fig 3f, g) without appreciable lag, suggesting high fidelity between pre- and post-synaptic measurements of DA release.

The nature of dopamine's influence in NAc is not fully understood, in part because distinct cell subpopulations express different DA receptors. We therefore tested whether Rdlight1 can simultaneously resolve DA fluctuations and the activity dynamics of genetically specified postsynaptic subpopulations, in behaving animals. We took advantage of a recently developed CRISPR knock-in rat that expresses Cre recombinase in D1- receptor expressing cells [23], and injected into the NAc both RdLight1 (AAV9-*CAG*-RdLight1) and Cre-dependent GCaMP6f (AAV5-*hSynapsin1*-FLEX-GCaMP6f; Fig. 3h, Extended Data Fig. 8). Once again, unexpected rewards were followed by increases in both signals, but this time there was a clear difference in time course (Fig. 3i). Session-wide, calcium in D1$^+$ cells was correlated with, but lagged behind, DA signals (Fig. 3j, k; peak cross-correlation = 0.54, at +372 ms).

Multiplexed measurement of dopamine and glutamate release *in vivo*

We next assessed our ability to study multiple, interacting neurotransmitters through the same optic fiber in behaving animals. The NAc receives glutamatergic input from multiple sources, and NAc DA terminals can also co-release glutamate[24], but the relative timing of DA and glutamate signals at fast timescales is unknown. In wild-type rats we co-injected RdLight1 (AAV9-*CAG*-RdLight1) and iGluSnFR (AAV1-*hSynapsin1*-iGluSnFR*)* into NAc, and chronically implanted an optic fiber (Fig. 4a, Extended Data Fig. 8). Aligned to an unpredicted reward cue, we again observed increased DA release (Fig. 4b, bottom); for glutamate we instead observed a strong decline in signal after a brief delay (Fig. 4b, top). DA increases to the reward cue were attenuated when the reward cue was partly predicted by preceding cues, as previously reported for dLight1 signals [1],[4]. Consistent with reward prediction error coding by DA [25], these preceding cues themselves evoked DA release, in proportion to the likelihood of reward that they signaled (Fig. 4c, bottom). These cues also produced glutamate dips that scaled with DA increases (Fig. 4c, top). The correspondence between fast DA increases and slightly delayed and slower glutamate dips is consistent with a known mechanism of DA action at D2 receptors on presynaptic glutamate terminals to

suppress release [26], but to our knowledge has not been previously reported in behaving animals.

In separate animals we performed two control experiments to exclude the possibility that decreases in iGluSnFR signals were the result of cross-talk caused by RdLight1 co-expression. First, we injected iGluSnFR alone (AAV1-*hSynapsin1*-iGluSnFR*)*, and again observed a decrease in NAc iGluSnFR signal in response to unpredicted reward cues (Extended Data Fig 9a–c). Next, we co-injected RdLight1 (AAV9-*CAG*-RdLight1) and a mutated iGluSnFR with ablated glutamate binding (AAV1-*hSynapsin1*-iGluSnFR(mut)*)* in NAc. This time, we again observed a robust increase in the RdLight1 signal, but no apparent increase in fluorescence intensity in iGluSnFR(mut) (Extended Data Fig 9d–f).

To provide additional support for these observations, and also begin distinguishing between distinct glutamate inputs to NAc, we expressed axon-targeted GCaMP6f (AAV1-*hSynapsin1*-axonGCaMP6f) in medial prefrontal cortex, then carried out simultaneous RdLight1 and GCaMP6f photometry in NAc (Fig 4d). We observed a very similar activity pattern in mPFC axons to the local glutamate dynamics described above (Fig 4e,f), indicating that mPFC terminals in NAc are participating in the general suppression of glutamate transmission that accompanies DA release after reward-predictive events.

Finally, we compared the peak signal-to-noise ratio (SNR) of RdLight1 to unpredicted rewards with green dLight1.3b which displays the highest dynamic range in dLight1 family. We noticed that the SNR of RdLight1 was significantly higher than that of dLight1.3b (~2 fold, $P = 8 \times 10^{-3}$, one-side t-test, Extended Data Fig. 10a). In addition, in a motivated behavior that is sensitive to NAc DA [39], the time taken to approach rewards did not differ between uninjected rats and those expressing either dLight1.1 or RdLight1 in the NAc (Extended Data Fig 10b), suggesting over-expression of RdLight1 does not appreciably affect NAc function in vivo.

Discussion

As the toolbox of genetically encoded optical sensors continues to grow, combining these tools becomes an increasingly powerful approach for dissecting information processing within brain circuits. To date, the useful red-shifted sensors for in vivo imaging are jRGECO and jRCaMP, which severely restricts the number of signaling events that can be studied simultaneously. Here we expanded the color spectrum of dLight1 by introducing two new spectral variants, the yellow YdLight1 and the red RdLight1. Though the utility of YdLight1 in multiplex imaging may be limited, it may be combined with scanned line angular projection microscopy for ultrafast imaging of DA release from cells in culture or in slice[27].

RdLight1 is a red genetically encoded membrane-integrated intensiometric sensor with a positive response and robust photostability and SNR *in vivo*. While existing red calcium sensors can be easily used for imaging of local neuronal activity (at the level of neuronal somata), their susceptibility to photobleaching compared to green calcium sensors [18,28] can present challenges under specific imaging conditions. For example, when distal neural projection activity needs to be measured together with local DA release, multiplexed use of

RdLight1 with a green calcium probe (e.g. GCaMP6f) is a valuable option. Furthermore, a red-shifted spectrum enhances SNR which is likely due to lower autofluorescence and increased imaging depth (Exteneded Data Fig. 10a).

How DA dynamics shape the activity of postsynaptic neurons is also a long-standing question [29]. Simultaneously monitor DA release (with RdLight) and calcium dynamics in D1+ neurons (with GCaMP6f) may spur broader application of multicolor photometry in behaving animals. In brain slices, DA increases excitability of D1+ striatal neurons [30]. Our working hypothesis is that the cue-evoked DA release makes D1+ neurons more responsive to excitatory glutamatergic inputs –particularly from sources such as medial frontal cortex [31] - and that these are ultimately responsible for driving the large increase in D1+ GCaMP signal we observed as the rats behaviorally responded to the reward cue. However, dual-color monitoring of RdLight1 and iGluSnFR revealed that reward-predictive cues provoke a marked decrease, rather than an increase, in glutamate release. We had expected to observe a fast glutamate increase, in part because such cues evoke rapid increases in spiking in many neurons within brain areas that provide glutamatergic inputs to NAc, including medial frontal cortex [32] and basolateral amygdala [33]. For this and other reasons, models of DA-glutamate interactions typically assume that salient cues evoke a strong glutamate increase in NAc, that would spill out of synaptic clefts [34]. Given the very limited spatial resolution of fiber photometry, our observation of a cue-evoked decrease in bulk extracellular glutamate suggests that the specific NAc glutamate synapses involved in evoking motivated behavior are relatively sparse with little spillover. This is in marked contrast to volume-conducted DA signals [35]. The rapid, widespread DA increase would presumably act on D2 receptors over a large proportion of glutamatergic synapses to produce the (slightly delayed) glutamate decrease we observed. The lack of a rapid cue-evoked glutamate increase is also noteworthy since many DA cells co-express glutamate as a neurotransmitter [24]. This may simply reflect our fiber placement in the NAc core, rather than the medial NAc shell which receives more joint DA and glutamate input [36]. Additional possibilities worth exploring are that the DA and glutamate-coexpressing neurons are preferentially unresponsive to cues, or that glutamate is not released during burst firing of DA neurons. Regardless, the ability to monitor DA and glutamate dynamics simultaneously in real-time –rather than on the multiple-minutes time scale of microdialysis –will be useful for investigating the interactions between these neurotransmitters, both in normal behaviors and in models of human disorders including drug addiction [37].

End users should first optimize the expression level of the sensor to be matched with imaging conditions in order to maximize SNR. Virus-mediated gene expression level varies depending on promoter, serotype and other conditions [38]. As dLight1-type sensors are based on inert GPCRs, their high affinity to endogenous ligands may be a double-edged sword. While one can be confident that the affinity is within the physiological range, overexpression of the sensor may buffer DA availability at endogenous DA receptors. In our specific experimental conditions, we demonstrated that dLight1-type sensors do not enage G-protein or beta-arrestin signaling in vitro. In addition, over-expression of RdLight1 and dLight1 does not appreciably affect NAc function in vivo (Extended Data Fig 10b). Neverthless, careful evaluation of the sensor's effect on signaling cascades, circuit activity, and behavior in other conditions and brain regions is needed for end users.

Since many new GPCR-based sensors are continuously introduced, such as GRAB-DA, GRAB-NE and GACh [2,40–41], RdLight1 opens doors to study neurotransmitter release and modulatory effects on neural circuits, and serves as an example for how to expand the color spectrum of GPCR-based sensors. Future engineering efforts are expected to improve sensor brightness and dynamic range (e.g. to assist two-photon imaging) and to further stretch the color palette (e.g. to far-red) [42–43], allowing even more signals to be monitored simultaneously.

Online Methods

Molecular Cloning

The red dopamine sensor library was generated using circular polymerase extension cloning (CPEC) [43]. pCMV.dLight1.3b was used as the destination vector, while the red fluorescent protein insert, containing circularly-permuted mApple and original linker sequences (see Extended Data Fig 1), was PCR-amplified from jRGECO1a. To generate sensor libraries the two amino acid-long linker regions on each side of cpmApple were then mutagenized with primers containing random codon sequences. BamHI and HindIII sites were introduced via PCR for final subcloning onto pAAV.hSynapsin1 and pAAV.CAG viral vectors. Single colonies were manually picked and grown overnight as described in [44]. All sensor sequences generated in this study are listed in the Supplementary Note Extended Data S1 file.

Structural modeling and sequence alignments

Active conformations of the sensors were predicted with rosetta_cm protocol of rosetta 3 (version 2015.31) [45]. The primary sequences of YdLight1 and RdLight1 were threaded with partial thread routine onto template PDB structures of active β_2AR [46] (ID: 3P0G) and Ca^{2+}-bound state of GCaMP3 [47] ID: 4IK3). The threaded structures were then hybridized together with rosetta_cm protocol for membrane protein [48]. A total of 10595 and 9828 PDB structures were generated by rosetta_script routine for YdLight and RdLight1, respectively. Structures with lowest total scores were considered the final models.

Cell culture, imaging and quantification

HEK293T cells (ATCC #1573) and U2OS cells (ATCC #HTB-96) were cultured and transfected as in [1]. Primary hippocampal and striatal neurons were freshly isolated and cultured as previously described [49,50]. Hippocampal neurons were virally transduced using AAVs (1×10^9 viral genomes/ml) at DIV5 two weeks prior to imaging. Striatal neurons were transfected via electroporation (Rat Neuron Nucleofector Kit; Lonza) per manufacturer's instructions. Immediately before imaging, cells were washed with HBSS (Life Technologies) supplemented with Ca^{2+} (2 mM) and Mg^{2+} (1mM). Cell imaging was performed using a 40X oil-based objective on an inverted Zeiss Observer LSN710 confocal microscope. The different color variants of the dopamine sensor were imaged using laser lines with the following wavelengths: 488 nm (dLight1.3b), 514 nm (YdLight1), 561 nm (RdLight1). For testing sensor responses, all neurotransmitters and drugs were directly applied to the bath during the imaging session. One-photon emission spectrum for the sensors was determined using the lambda-scan function of the confocal microscope and the following laser lines: 488 nm for dLight1.3b and YdLight1, 561 nm for RdLight1. Surface

labeling using anti-flag antibody was achieved as described previously [51]. For ROIs selection, masks were generated on individual cell membranes using the threshold function in Fiji (Image J). For titration curves, apparent K_d values were obtained by fitting the data with a One-site specific binding function on GraphPad Prism 6. We calculated spatial movies and images of F/F in response to an applied ligand as $(F(t) - F_0)/F_0$ with $F(t)$ being the pixel-wise fluorescence value at each time, t, and mean fluorescence in time points prior to ligand application, F_0. To avoid the possibility of infinite pixel values, we added a small offset to each pixel in F_0. Based on the F/F maps, we calculated a corresponding SNR map as $\Delta F/F \times \sqrt{F_0}$. Heatmaps were generated using a custom-made MATLAB script.

When perfusion is performed, 20x objective was used. Imaging setting was kept constant across all the samples. ligands (DA or NE) were diluted to 1 μM in HBSS with 2 mM $CaCl_2$ and 1 mM $MgCl_2$ (HBSSCaMg). Perfusion while imaging was done on RC-48LP low profile open bath chambers (Warner Instruments, Hamden, CT). 5 ml of HBSSCaMg was used to flow through before and after 5 ml 1 μM ligands in HBSSCaMg. For FACS analysis, the cells were lift and basal fluorescence intensity were measured on BD FACScan cytometer. Both were excited with 488 nm laser, green channel emission filter is 530/30 bandpass filter, and red channel is 585/42 bandpass filter. Data was analyzed with flowCore package (Ellis B, Haaland P, Hahne F, Le Meur N, Gopalakrishnan N, Spidlen J, Jiang M, Finak G (2019). flowCore: flowCore: Basic structures for flow cytometry data. R package version 1.52.1.) in Bioconductor.

Internalization assay with flow cytometry

24 hours post transfection, cells were re-plated onto 6-well dishes. The following day, surface levels of receptors were assayed by addition of Alexa-647-conjugated M1 antibody (Sigma) for 45 minutes, as described previously [51]. Fluorescence intensity profiles of cells populations (>5000 cells) were measured using a FACS-Calibur instrument (BD Biosciences). Each condition was performed in duplicate. Internalization was calculated by measuring the fraction of surface fluorescence remaining after 30 minutes of 1 μM SKF81297 (Tocris) and divided by the non-treated condition.

Luminescence and fluorescence-based cAMP assays

Luminescence experiments were conducted as previously described [51]. Briefly, cells were transfected with the cyclic-permuted luciferase pGLOSensor-20F plasmid (Promega) 34 hours before the experiment, and then treated with luciferin (GoldBio) in phenol red and serum-free DMEM for 1 hour in a 24 well dish. The indicated conentrations of SKF81297 (Tocris) were added and luminescence values were measured at peak using a plate luminometer at 37°C. Then 10 μM forskolin (Sigma) was added and the peak luminescence value was measured to normalize the SKF81297 response across wells. Fluorescence measurements of cAMP accumulation in cultured striatal neurons were performed using a green genetically encoded cAMP sensor expressed by a CAG promotor-driven baculovirus vector (Green Up cADDis, Montana Molecular) [52], and achieving co-expression of RdLight1 by coinfection with AAV. Cells were imaged using an inverted spinning disk confocal microscope and 60x NA1.4 oil-immersion objective. 488 nm laser illumination was used to excite the cAMP sensor, 561 nm illumination was used to excite intrinsic RdLight1

fluorescence, and 561 nm illumination was used to excite Alexa647-conjugated anti-Flag monoclonal antibody detecting surface expression of RdLight1. Kinetics of the cAMP response were determined by sequential imaging at 37°C, with SKF81297 bath applied at 1 μM, and with 10 μM forskolin added at the end of the acquisition series to normalize responses across neurons.

Total Internal Reflection Fluorescence Microscopy (TIRF-FM) Live Imaging.

Live cell TIRF-FM was conducted with a Nikon Ti-E inverted microscope at 37°C in a controlled humidity and CO2 controlled chamber as described previously [51]. D1 specific agonist SKF81297 (Tocris) was added at 1 μM while D1 antagonist SCH23390 (Tocris) was added at 10 μM.

AAV viral production

All RdLight1 AAV constructs were cloned in the laboratory. RdLight1 and axon-GCaMP6f viruses were produced by the UC Davis Vision Center Vector Design and Packaging Core facility. The viral titers of the viruses used in this study were: AAV9.*CAG*.RdLight1, ~1 × 10^{12} GC/mL; AAV9.*hSynapsin1*.RdLight1, ~1 × 10^{12} GC/mL; AAV1.*hSynapsin1*.GCaMP6s, ~1 × 10^{12} GC/mL; AAV9.*CAG*.Flex.GCaMP6f, ~1 × 10^{12} GC/mL; AAV5.*hSynapsin1*.iGluSNFR, ~2.9 × 10^{12} GC/mL; AAV1.*hSynapsin1*.axon-GCaMP6f, ~1 × 10^{12} GC/mL.

Animals

Animal studies were conducted in compliance with the Guide for the Care and Use of Laboratory Animals of the National Institutes of Health and approved by the Institutional Animal Care and Use Committee (IACUC) at the University of California, Davis or the relevant institutional regulatory body.

Viral injections

Injection procedures were essentially identical to those described in [1] with a few exceptions. For dopamine, glutamate, and calcium imaging in brain slices, male and female C57/Bl6 mice (8–12 weeks old) were used for intracerebral microinjections. Briefly, anesthetized mice were immobilized in a Stereotaxic Alignment System (Kopf Instruments). AAV9.*hSynapsin1*.RdLight1 alone or mixed at 1:1 ratio in combination with either AAV5.*hSynapsin1*.iGluSNFR or AAV9.*hSynapsin1*.GCaMP6s was injected undiluted at a total volume of 150 nl uni-laterally into the dorsal striatum using the following coordinates from bregma (in mm): 0.8 anteroposterior (AP), ±1.5 mediolateral (ML), −3.2 dorsoventral (DV).

Slice preparation and ex vivo two-photon imaging

2–4 weeks after viral injection, mice were anesthetized with 2.5% avertin and decapitated. The heads were placed in high-sucrose artificial cerebrospinal fluid (aCSF) that contained (in mM): 73 NaCl, 2.5 KCl, 2 $MgCl_2$, 1.25 NaH_2PO_4, 25 $NaHCO_3$, 24 dextrose, 0.5 $CaCl_2$ and 75 sucrose, 300 mOsm, saturated with 95% O_2 and 5% CO_2. The brains were then removed from the skull and cut (400 μm) with vibratome (V1200s, Leica) in ice-cold high-

sucrose aCSF. Brain slices were incubated at 32ºC for 30 min in normal aCSF that contained (in mM): 128 NaCl, 2.5 KCl, 1 $MgCl_2$, 1.25 NaH_2PO_4, 25 $NaHCO_3$, 10 dextrose and 2 $CaCl_2$, 300 mOsm, saturated with 95% O_2 and 5% CO_2. After incubation, slices were placed in aCSF at room temperature for 30 min before imaging. Imaging was carried out in a 2-photon microscope with a heated slice perfusion system enabling recordings at 37ºC. Fluorescence of both green and red indicators was excited at 1020 nm with a Ti: sapphire laser (Ultra II, Coherent) that was focused by an Olympus 40×, 0.8NA water immersion objective. Emitted light from the two indicators was separated using the following filter sets: 525/50nm and 620/60nm. Data were acquired and collected with ScanImage5 software. Electrical stimulation was performed by placing a metal bipolar electrode (PI2ST30.01A5, Microprobes for life science) within the slice approximately 50 μm away from the area of imaging. Different number of pulses of identical amplitude and duration (4 V, 0.5ms each) were applied though a Grass SD9 stimulator. Triggers for imaging and electrical stimulation were controlled by Axon Digidata 1550B. Experiments were carried out with a scan rate of 198 (64×64 pixels) or 30 (512×512 pixels) Hz. The fluorescence over the entire field (7.5×7.5 μm for 198 Hz, 60×60 μm for 30 Hz) was measured for each frame and plotted against time. Drugs were dissolved as a stock solution either in dimethyl-sulfoxide (DMSO) or in aCSF, and diluted at least 1:10,000 prior to application in the perfusion system. Image analysis was performed with ImageJ and curve fits and data analyses were calculated using OriginPro 8.0 and SigmaPlot 12.0. Electric stimulation in different situations (without or with drug) was repeatedly applied 3 times (20-s interval) on each slice. Overall fluorescence of whole frame was analyzed and averaged to improve signal to noise ratio (SNR). Grey trials in Figure 2 show the average results from all slices. Tau_{on} was calculated by fitting the fluorescence rise with a linear regression and Tau_{off} was calculated by fitting the fluorescence decay with a single exponential curve. Inset shows zoomed-in view of the fluorescence peak.

Two-photon bleaching measurements

Two-photon bleaching measurements of RdLight were acquired from acute brain slices. Laser excitation was at 1020 nm and focused by an Olympus 40×, 0.8NA water immersion objective. Emitted fluorescence photons were separated by a 620/60 nm filter. Scan area was 60 μm×60 μm, and the scan rate was 30 frames/s. Light intensity was kept at 8.7 mW across measurements. Burst electrical stimulation was performed with a metal bipolar electrode (PI2ST30.01A5, Microprobes for life science) every 100 s. Amplitude of the pulses was 4 V, width was 0.3 ms and a total number of 40 pulses was applied at a frequency of 80 Hz.

Histology and confocal imaging

Mice were deeply anesthetized with 2.5% avertin and transcardially perfused with 10 mL 1× Dulbecco's phosphate buffered saline (DPBS, Gibco), followed by 50 mL 4% paraformaldehyde in DPBS. After perfusion, the brains were removed and post-fixed overnight at 4°C. The brains were embedded in 5% sucrose in DPBS overnight at 4°C, and then embedded in 15% sucrose in DPBS for 48 h. Fixed brains were cut into 30 μm thick coronal sections with a vibratome (Leica CM 3050S, Germany). Sections were coverslipped with mounting medium (ProLongTM Glass Antifade Mountant, Thermo Fisher Scientific). Confocal images (LSM 710, Zeiss) were collected using a 40×, 1.3NA oil objective. Emitted

light was separated using the following filter sets: 488nm and 561nm. Data were acquired with Zen software and analyzed with ImageJ.

In vivo fiber photometry

We used a viral approach to express different genetically encoded indicators and actuators in the brain. We injected 1μl of AAV1-*hSynapsin1*-FLEX-axon-GCaMP6f or AAV5-*EF1a*-FLEX-ChR2-eYFP slowly into the lateral VTA (AP:−5.7, ML:0.9, DV:−7.5mm) and AAV9-*CAG*-RdLight1 or AAV9-*hSynapsin1*-iGluSnFR into the ventral striatum (AP:1.7, ML:1.7, DV:−7.0mm). During the same surgery, a 400μm core optical fiber was implanted 200um above the injection site and anchored to skull using dental cement. For GCaMP6f, we used a 470nm blue excitation LED (Thorlabs) and 405 nm violet for isosbestic control, modulated at different frequencies (211Hz and 531Hz). We used a 565 nm red-shifted LED to excite RdLight1 at 340Hz frequency. All three excitation signals were passed through a 6-port filter cube (Doric) and emission signals were amplified using a picowatt amplifier (Newport, model 2151) and saved on the disk using a Labview based data acquisition system. Output of the amplifiers were demodulated offline to separate the indicator and control responses.

All photometry recordings were done in operant training chambers (Med Associates; 25cm x 30cm), with five nosepoke ports and a food retrieval cup with houselight on. Rats were mildly food deprived (receiving 15g of standard laboratory rat chow daily) and received between 5–8 training sessions before the experiment. Each session consisted of 60 trials of each of: unpredictable rewards; cues predicting reward with 75% probability; and cues predicting reward with 25% probability, randomly interleaved, with random inter-trial-intervals (15–30s, uniform distribution). Cues were trains of auditory tone pips (2KHz or 9 KHz, 100ms on, 50ms off), associated with 75% or 25% chance of reward delivery 2.8 s after cue onset, as in ref. (*4*).

Statistics and reproductivity

All statistical analyses were performed in MATLAB (MathWorks R2017a), Igor Pro (WaveMetrics) or Prism (GraphPad). For determining statistical significance we used either parametric (paired t-test, one-way ANOVA) or non parametric tests (Kolmogorov-Smirnov test). All tests were two-tailed. Error bars are standard error of the mean or standard deviation as indicated in figure legends and main text. No statistical methods were used to predetermine sample size. When representative images and micrographs or single-trial fluorescence responses are shown, experiments were performed either at least three times or across many trials (trial numbers are stated in the figure legends) unless otherwise noted.

Further information on research design is available in the Nature Research Reporting Summary linked to this article.

Extended Data

Question	Approach	Results	Figures

Sensor Engineering

A. Can we design a red-shifted DA sensor?

B. What are the properties of RdLight1?

→ Replacing cpGFP with cpmApple in dLight1.1 followed by linker screening and loop mutation to optimize sensitivity

→ Intrinsic properties similar to dLight1.1
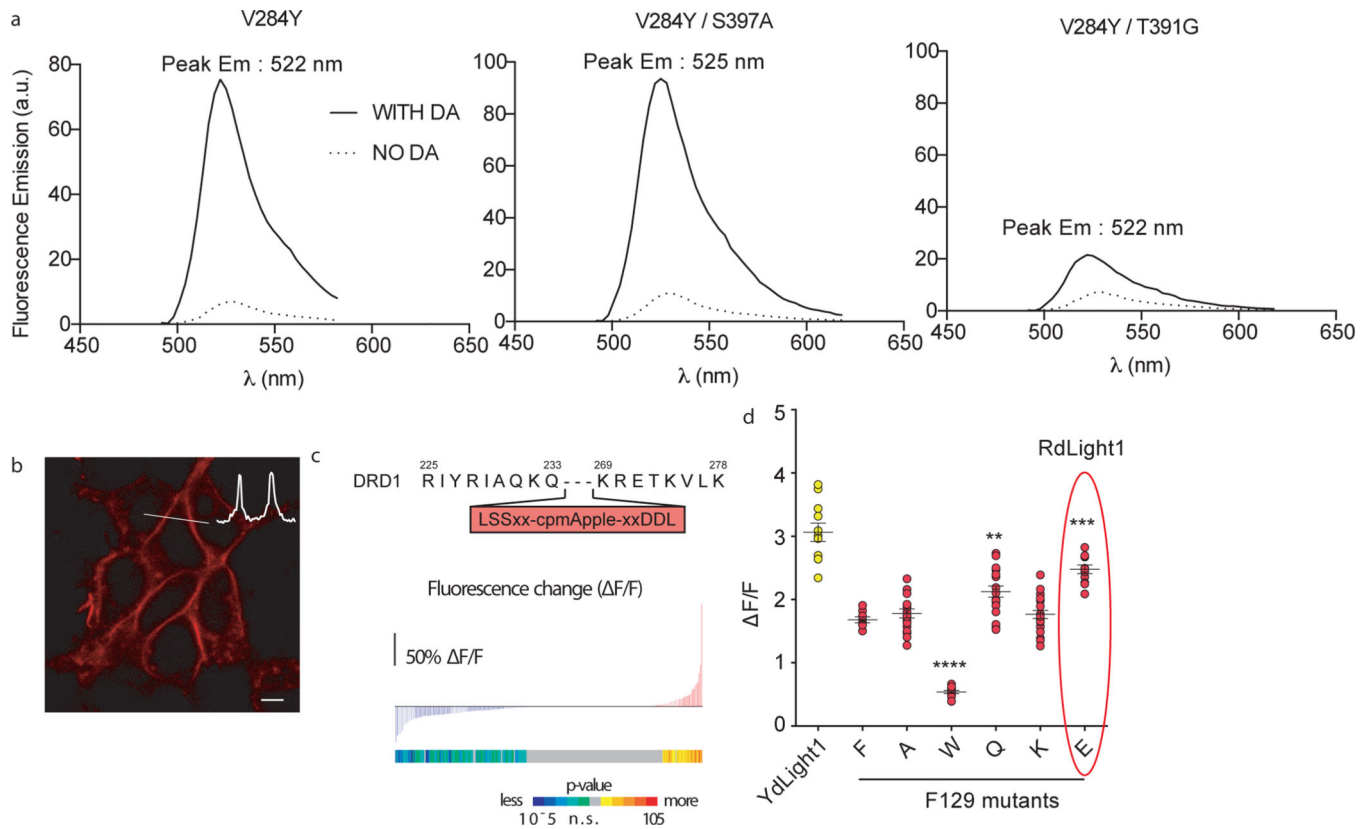peak emission 588nm
membrane expression
apparent Kd = 229 nM in neurons
$\Delta F/F = 250\%$
~60-fold more sensitive to DA than NE in neurons → Fig. 1a-d
Does not engage G-proteins
Does not internalize
Photostability permits longitudinal imaging in vivo → Fig. 3g

Dual color imaging in cells

C. Can we image drug target engagement with two different G-protein coupled receptors (GPCRs) in the same assay?

→ Combine two distinct GPCR sensors (DRD1 and DRD2-based) with orthogonal emission wavelengths

→ Potency and efficacy of DRD1 and DRD2 selective agonists could be determined in a single assay → Fig. 1e-f

D. Can we image DA and NE simultaneously?

→ cell-type specific labeling of neuron and astrocytes with RdLight1 and nLight1.3

→ cell-type specific responses to bath-applied DA or NE which can be blocked with Receptor-specific antagonists → Fig. 1g-h

Two-photon dual color imaging in striatal slice

E. Can we simultaneously image the dynamics of DA and glutamate or calcium in striatum?

→ 1. Co-express iGluSNFR or GCaMP6f with RdLight1 in the mouse brain
2. Perform dual-color imaging in slices with two-photon microscopy

→ Electrical stimuli or drug application lead to different effects on the kinetics of glutamate or calcium and dopamine release. → Fig. 2

Multi-color fiber photometry imaging of DA and cell-type specific calcium activity

F. Can RdLight1 detect light-evoked DA transients in vivo?

→ Express RdLight1 in NAc and ChR in VTA followed by optical stimulation

→ RdLight 1 can resolve individual peaks up to 8 Hz → Fig. 3a-b

G. Can we monitor DA release together with cell-type specific input or output activity in vivo?

→ 1. Label VTA projections with Flex-axon-GCaMP6f and RdLight1 in NAc of TH-Cre rats
2. Perform dual color photometry imaging in the NAc to reward
3. Label D1-MSNs with GCaMP6f and RdLight1 in NAc of DRD1:Cre rats
4. Perform dual color photometry imaging in the NAc

→ Strong correlation of VTA presynaptic calcium with DA release in NAc in response to reward → Fig. 3d-g

Calcium activity in D1-MSNs is correlated but lags behind DA transients in reponse to reward → Fig. 3h-k

Multi-color fiber photometry imaging of DA and glutamate

H. Can we monitor the dynamics of two neurotransmitters during reward-seeking behavior?

→ 1. Express RdLight1 and iGluSnFR in NAc followed by dual color photometry
2. Label mPFC projections with GCaMP6f and express RdLight1 in NAc followed by dual color photometry

→ Dichotomy between accumbal dynamics of glutamate and dopamine to reward-predicting cues → Fig. 4a-c

mPFC projections participate to global glutamate reduction in NAc during reward-predicted cues → Fig. 4d-f

Extended Data Fig. 1. Outline and summary of the experiments.
Outline and summary

Extended Data Fig. 2. Development of RdLight1.
a, Fluorescence emission spectra of dLight1.3b variants carrying red-shifting mutations in their GFP component. Fluorescence emission was measured in the 450–650 nm wavelength range both in the absence of DA (dotted lines) and upon addition of 100 μM DA to the medium (continuous lines). n = 4 cells from 3 cultures. **b**, Representative image showing membrane expression profile of the initial variant of the red dopamine sensor, carrying the original amino acid linkers from JRGECO1a. The experiments were repeated at least twice with similar results. **c**, linker screening results from a library of 264 variants in which the two aminoacid pairs flanking cpmApple were randomized (as shown in inset). Red and blue vertical bars indicate fluorescence changes (F/F) in response to 100 μM DA; significance values of F/F are shown by colored bars and scale. n = 3 trials, two-tailed t test. **d**, optimization of the RdLight1 fluorescence response was achieved by selectively mutating residue F129 into a subset of amino acids. Fluorescence change (F/F) was measured in HEK293 cells in response to bath-applied 100 μM DA. n = 4 cells from 2 cultures. **p<0.01, ****p<0.0001, two-tailed t test. The experiments were repeated at least twice with similar results. Data are shown as mean ± SEM.
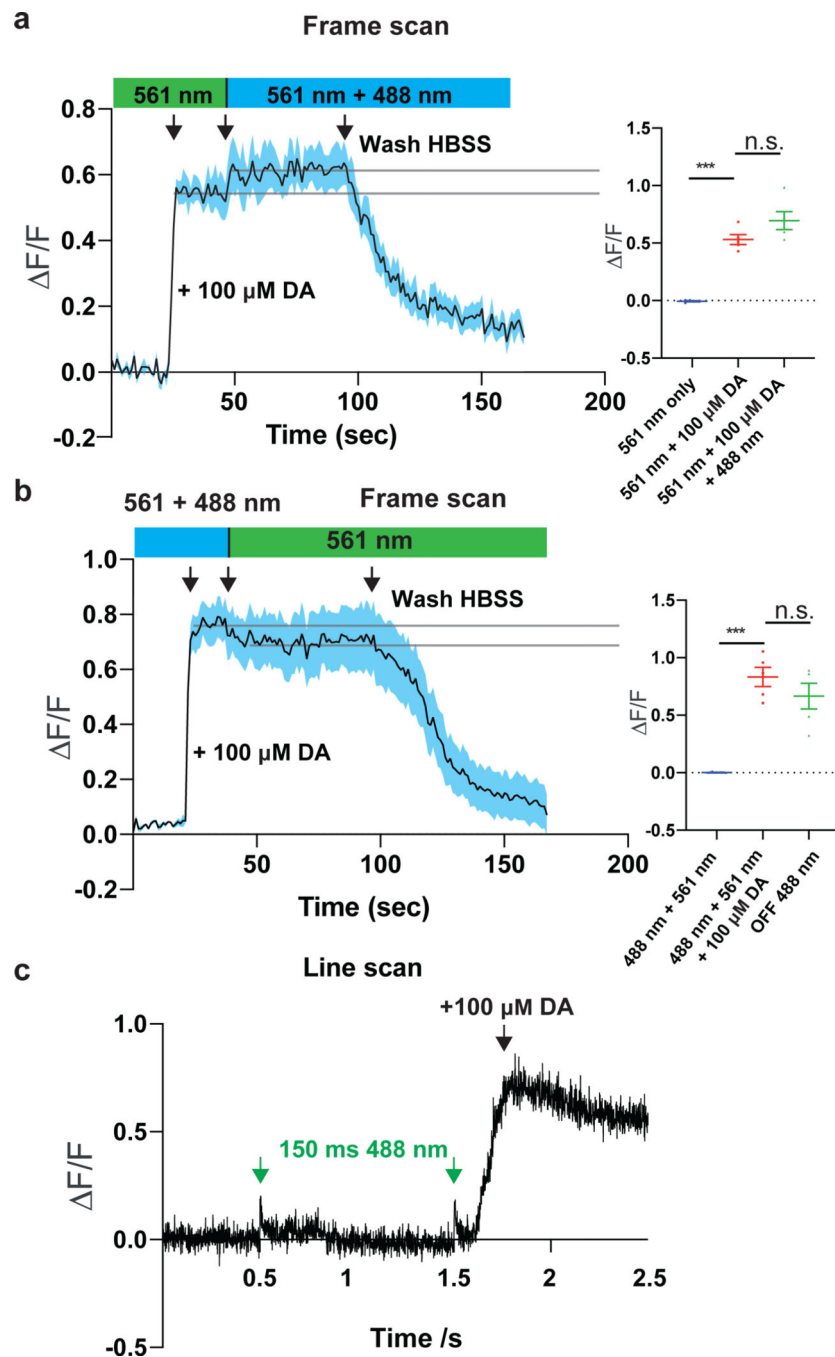
Extended Data Fig. 3. Characterization of RdLight1 photoactivation by blue light.
Confocal imaging of RdLight1 in transfected HEK293 cells. **a-b** Frame scan imaging
performed in the presence of both blue (488 nm) and green (561 nm) light after (a) or before
(b) bath-application of DA. Blue light did not significantly increase the fluorescence
response of RdLight1 to DA. Average F/F=−0.006±0.003 (baseline), 0.53±0.03(DA),
0.69±0.06(DA+blue light, One-way Anova, ***P=0.0005, n.s P=0.1224, n=5 cells from two
cultures (**a**). Average F/=0.002±0.001 (baseline+blue light), 0.83±0.06(DA+blue light),
0.69±0.08(DA), One-way Anova, ***P=0.0007, n.s P=0.0678, n=5 cells from two cultures,

mean±SEM (**b**). **c**, Representative line scan imaging at acquisition rate of 1000 Hz. Bursts of 488nm laser (150 ms duration at 1Hz) was applied followed by application of DA. Laser powers used were: 24779.4 W/cm^2
for 561nm laser, 16373.7 W/cm^2 for 488nm laser. Experiments were performed six times with similar results.
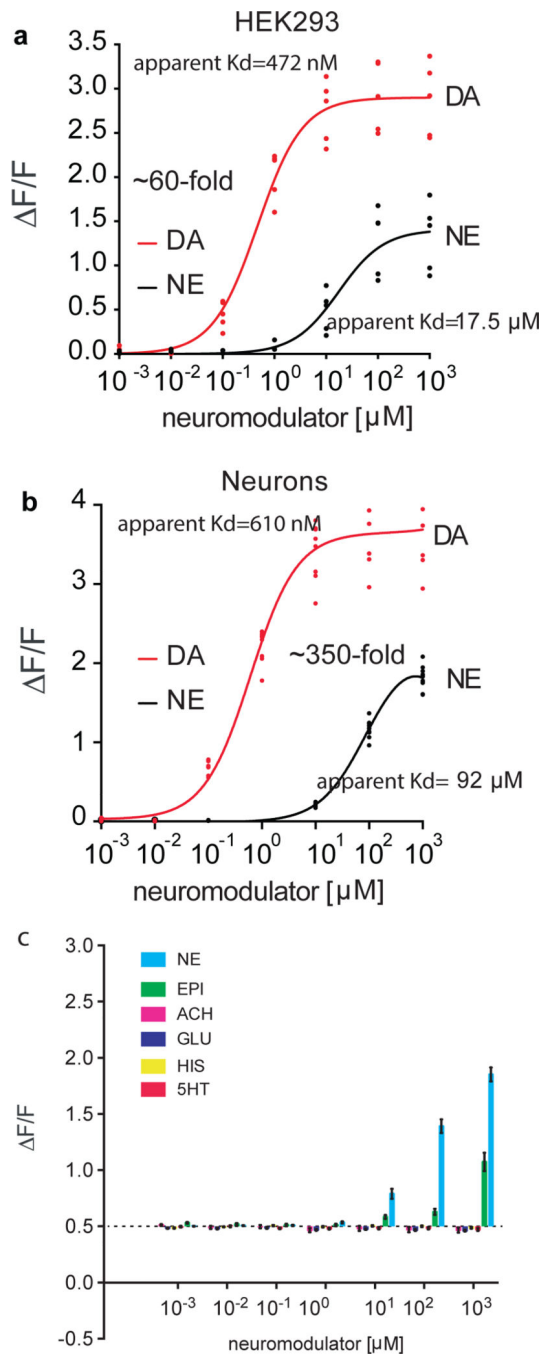
**Extended Data Fig. 4. Molecular specificity of RdLight1.**

a-b, Titration curves are shown for the response to DA or NE both in HEK293 cells and in cultured neurons. Data points were fit with a one-site specific binding curve to obtain EC_{50} values. Data are shown as mean ± SEM. n = 7 cells from 2 cultures for both HEK293 cells and neurons. The response of RdLight to NE at 1mM is significantly lower than that to DA ($P=4.8\times10^{-8}$, paired t-test (two sided). **c**, The specificity of RdLight1 was tested by performing titrations of a panel of different neurotransmitters on the sensor expressed in HEK293 cells. Quantification of responses to each concentration of ligand are shown as mean ± SEM. n = 12 cells from 2 cultures. Neurotransmitters tested were: norepinephrine (NE), epinephrine (EPI), acetylcholine (ACH), glutamate (GLU), histamine (HIS), serotonin (5HT). The experiments were repeated at least twice with similar results.
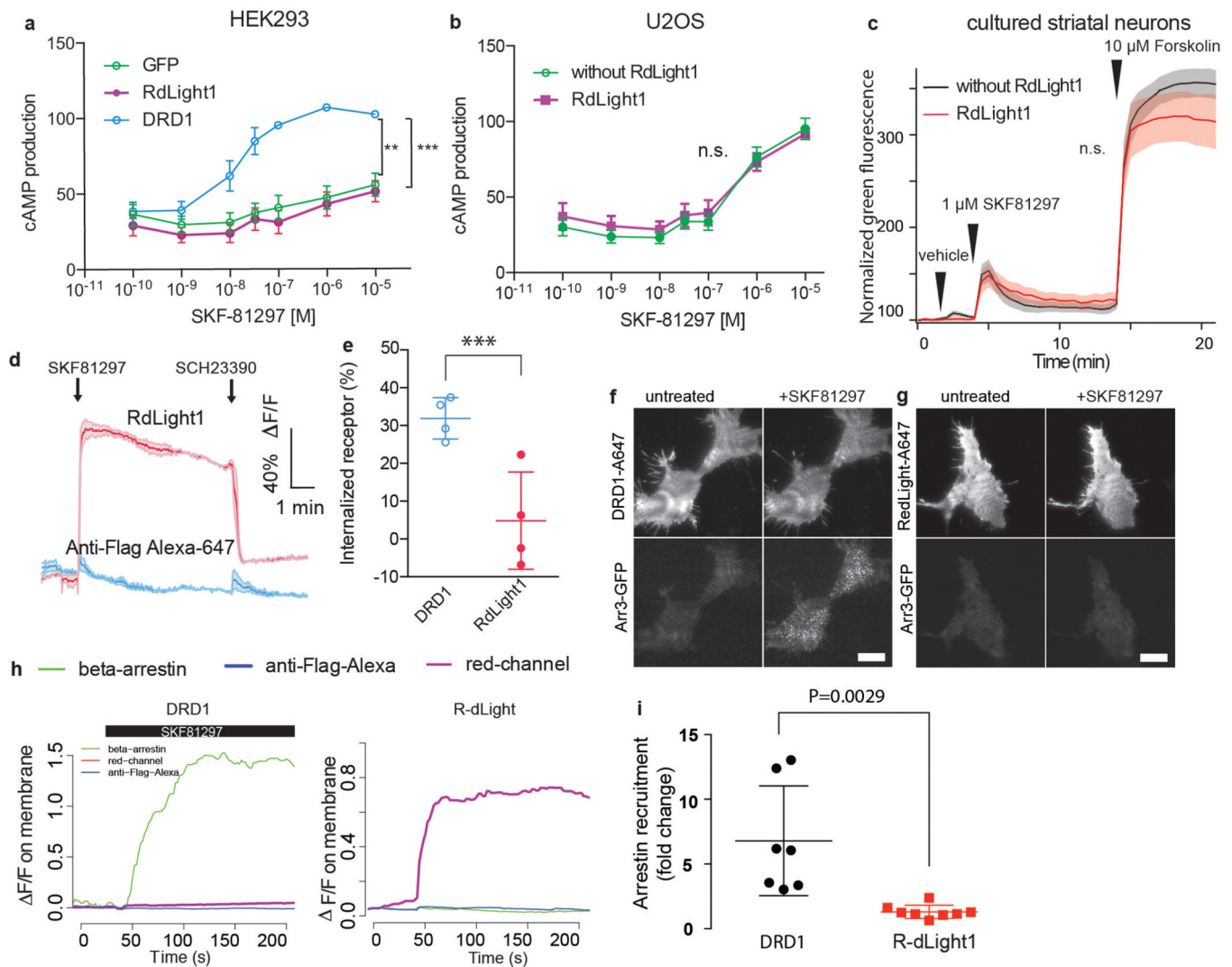
Extended Data Fig. 5. Cellular signaling characterization of RdLight1.
a, cAMP response curve to a titration of the D1 agonist SKF81297 in HEK293 cells transfected with RdLight1 compared to human D1-dopamine receptor (DRD1, positive control) or enhanced green fluorescence protein (GFP, negative control). No significant cAMP response was produced by RdLight1 (n=3 independent experiments, **p=0.0033,

***p=0.00053, one-way ANOVA, Dunnett's post-hoc test). **b**, cAMP response curves of a cell line endogenously expressing DRD1 (U2OS). Overexpression of RdLight1 did not alter the endogenous cAMP response to SKF81297 (n=3 independent experiments, p=0.944, two-way ANOVA). **c**, Expression of RdLight1 (red) in cultured primary striatal neurons did not affect cAMP responses to vehicle, SKF81297 or the adenylate cyclase activator Forskolin, compared to mock-transfected conditions (black), as measured by the green genetically encoded cAMP sensor cADDis (n=10 neurons from three cultures, P=0.744 (unpaired t-test, two-tailed). **d**, TIRF imaging of RdLight1 response (red) and of a static Alexa-647-conjugated anti-Flag antibody label to delineate sensor expression on cell surface (far-red channel). Quantification of RdLight1 response to a DRD1 agonist (SKF81297), which was immediately abolished by applying antagonist (SCH23390) (n=3 independent experiments). **e**, RdLight1 internalization is significantly reduced compared to wild type DRD1 as assayed via flow cytometry (% internalized receptor: RdLight1, 4.82 ± 6.42 %; DRD1, 31.9 ± 2.74 %, n=4 independent experiments, p=0.0006 (unpaired t-test, two-tailed). **f-g**, Representative TIRF microscopy images of HEK293 cells transfected with beta-arrestin-2 and DRD1 or RdLight1. DRD1 and RdLight1 were labeled with an Alexa-647 conjugated anti-flag antibody. Conditions before and after addition of DRD1 agonist SKF81297 are shown. Experiments were performed three times with similar results. **h-i**, Quantification of beta-arrestin-2 recruitment on the cell membrane from **f-g**. Under these conditions RdLight1 triggers significantly lower beta-arrestin-2 recruitment than DRD1. RdLight1, 6.8 ± 4.2 (n=8 cells); DRD1, 1.3 ± 0.5 (n=7 cells), P=0.0029 (unpaired t-test, two-tailed). All values shown are mean±SD.
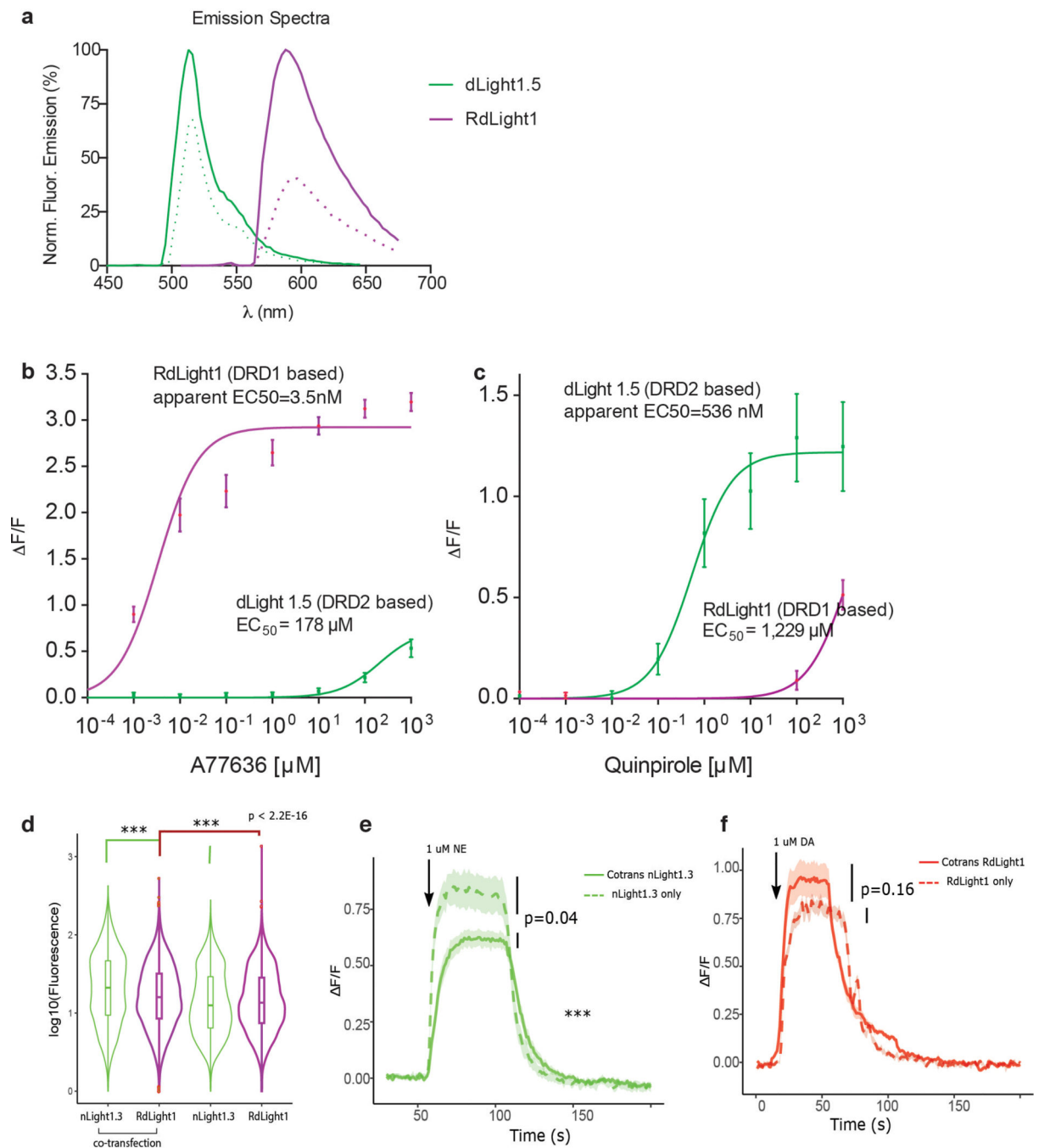
Extended Data Fig. 6. Multiplex imaging of drug selectivity at two dopamine receptor subtypes and characterization of RdLight1 and nLight1.3 coexpression.

a, Combined fluorescence emission spectra of DRD1-based (dLight1.5) and DRD1-based (RdLight1) sensors used for multiplex imaging experiments. Fluorescence emission was measured in the 450–700 nm wavelength range both in the absence of DA (dotted lines) and upon addition of 100 μM DA to the medium (continuous lines). n = 4 cells from 3 cultures. **b-c**, Dose-response curves were obtained by performing multiplex imaging during titrations of the DRD1-selective agonist A77636 or the DRD2-selective agonist Quinpirole on a
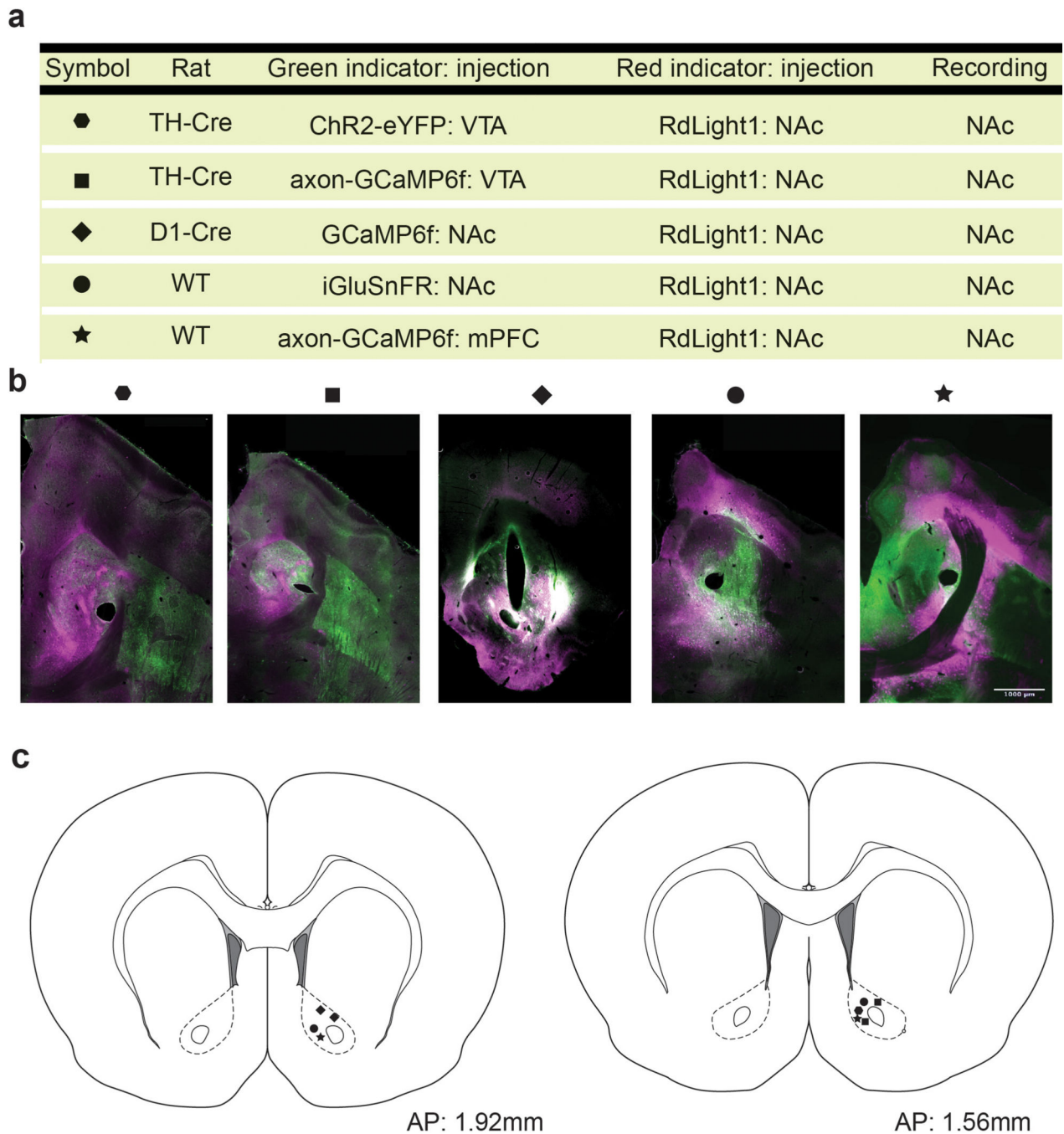
coculture of two HEK293 cell populations expressing either RdLight1 (red) or dLight1.5 (green). Maximal fluorescence responses at each applied concentration were quantified and plotted. n = 6 cells from 3 cultures. Data are shown as mean ± SEM. **d-f**, Characterization of RdLight1 and nLight1.3 coexpression. **d**) Flow cytometry analysis of cells transfected with RdLight1 (n=13928 cells), nLight1.3(n=25798 cells), or both (n=33049 cells) showed that co-transfection significantly increased both basal green and basal red-fluorescence. Violin plots show the distribution of the log value of fluorescence, on top of the boxplot of the same data. P=2.2X10^{-16} Two-sided Student's t-test. **e, f**. In a perfusion experiment, confocal time-lapse imaging revealed that the response of nLight1.3 to NE when expressed alone (n=8) can be slightly decreased when cotransfected with RdLight1 (n=7 cells), which could possibly due to increased basal green fluorescence from RdLight1 co-transfection. A slight increase in the amplitude of response in RdLight1 was noticed when co-transfected (n=7 cells), but not significant. P=0.04 and 0.16, Two-sided Student's t-test for the value when NE or DA applied. Traces were plotted as mean +/− sem, with center line as mean value and shade the s.e.m.
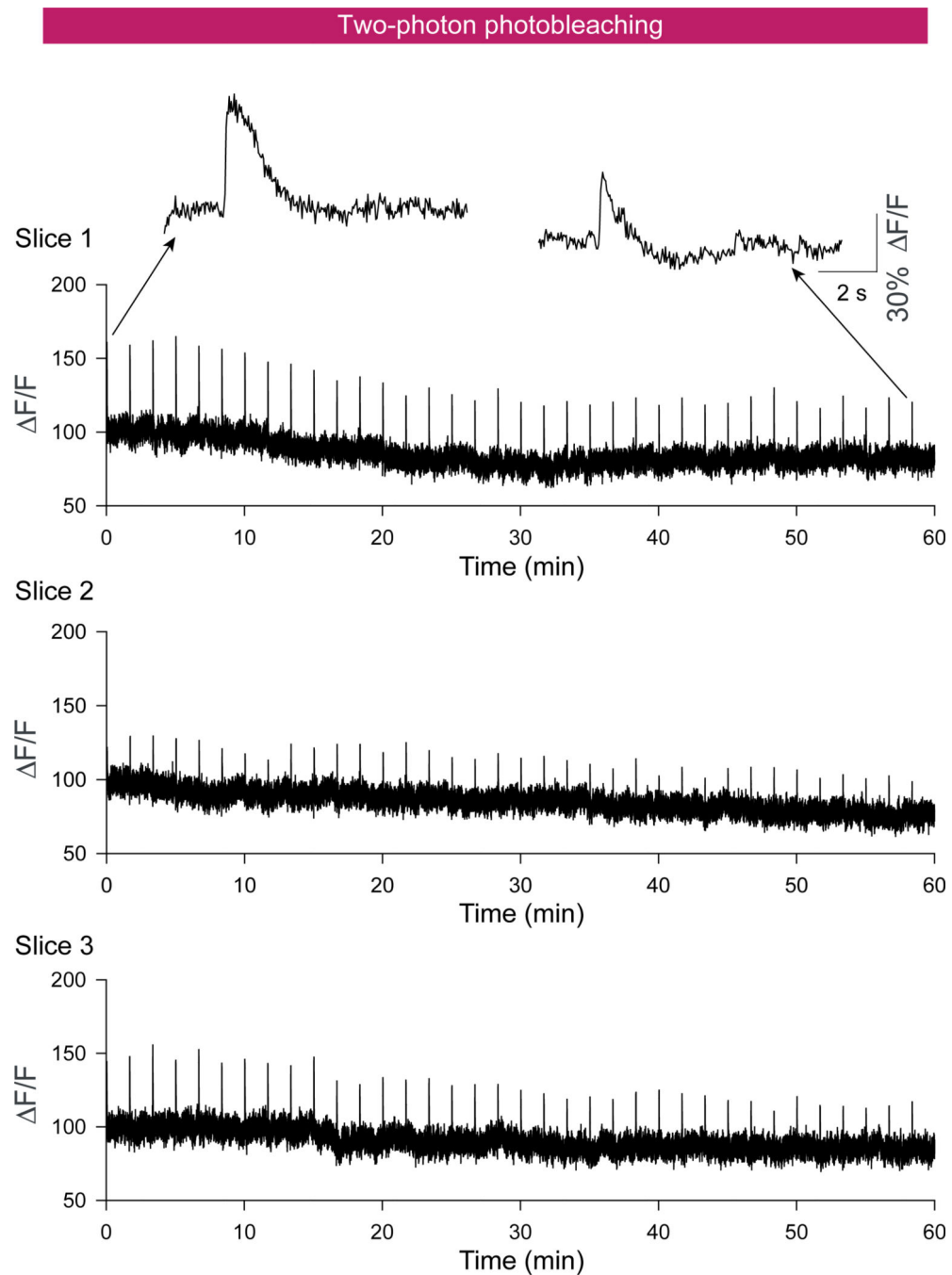
Extended Data Fig. 7. Photobleaching of RdLight1 under two-photon illumination.
Two-photon bleaching measurements of RdLight were acquired from acute brain slices.
Fluorescence of RdLight was excited at 1020 nm with a Ti: sapphire laser (Ultra II,
Coherent) that was focused by an Olympus 40×, 0.8NA water immersion objective. Emitted
fluorescence photons were separated by a 620/60 nm filter. Scan area was 60 μm×60 μm,
and the scan rate was 30 frames/s. Light intensity was kept at 8.7 mW across measurements.
Burst electrical stimulation was performed with a metal bipolar electrode that has a tip
spacing of 255 μm (PI2ST30.01A5, Microprobes for life science) every 100 s. Amplitude of

the pulses was 4 V, width was 0.3 ms and a total number of 40 pulses was applied at a frequency of 80 Hz. As shown in the figure, photobleaching was continuously measured in a 1 h duration. Overall fluorescence in all the 3 tested slices declined about 17.2±3.1%, mean ± SEM. The experiments were repeated in 3 slices from two mice with similar results.

a

Symbol	Rat	Green indicator: injection	Red indicator: injection	Recording
⬟	TH-Cre	ChR2-eYFP: VTA	RdLight1: NAc	NAc
■	TH-Cre	axon-GCaMP6f: VTA	RdLight1: NAc	NAc
◆	D1-Cre	GCaMP6f: NAc	RdLight1: NAc	NAc
●	WT	iGluSnFR: NAc	RdLight1: NAc	NAc
★	WT	axon-GCaMP6f: mPFC	RdLight1: NAc	NAc

b

c

AP: 1.92mm   AP: 1.56mm

Extended Data Fig. 8. Injection coordinates for in vivo experiments.
a, List of all in vivo experiments in which RdLight1 was expressed in NAc simultaneously with a green indicator. **b,** Representative stitched image for each experiment collected on an

epifluorescence microscope using a 4x objective. All sections (except for the *D1-Cre* example) are collected in horizontal planes. The *D1-Cre* example is in the coronal plane. Each section shows the most ventral section with a fiber punch hole. Scale bar: 1 mm. **c,** Overlaid reconstruction map of the estimate location of recordings for each experiment. Histology results were not available for one subject in the *TH-Cre* experiment since the subject died prior to the end of the experiment. Brain atlas outlines in this figure were reproduced with permission from (Paxinos and Watson, 2005).

Extended Data Fig. 9. Additional control experiments for in vivo imaging with iGluSnFR.
To further validate the dip observed in the glutamate signal in NAc following the reward click in Fig 4, we performed two complementary experiments. **a** Only iGluSnFR was expressed in NAc and imaged using a 400 μm fiber during the pavlovian approach task. **b-c,** similar patterns to Fig 4b,c, demonstrating a dip following the reward click was observed when only iGluSnFR was expressed and monitored. **d-f,** To control for pH changes or other artifacts, we expressed a variant of iGluSnFR (SF-iGluSnFR.R75A) with a mutation to the binding sites that destroyed glutamate binding, along with RdLight1. While similar to Fig

4b,c RdLight1 signal was preserved, the dip in the glutamate signal disappeared. Experiments for each panel were repeated independently for n=2 rats with similar results.
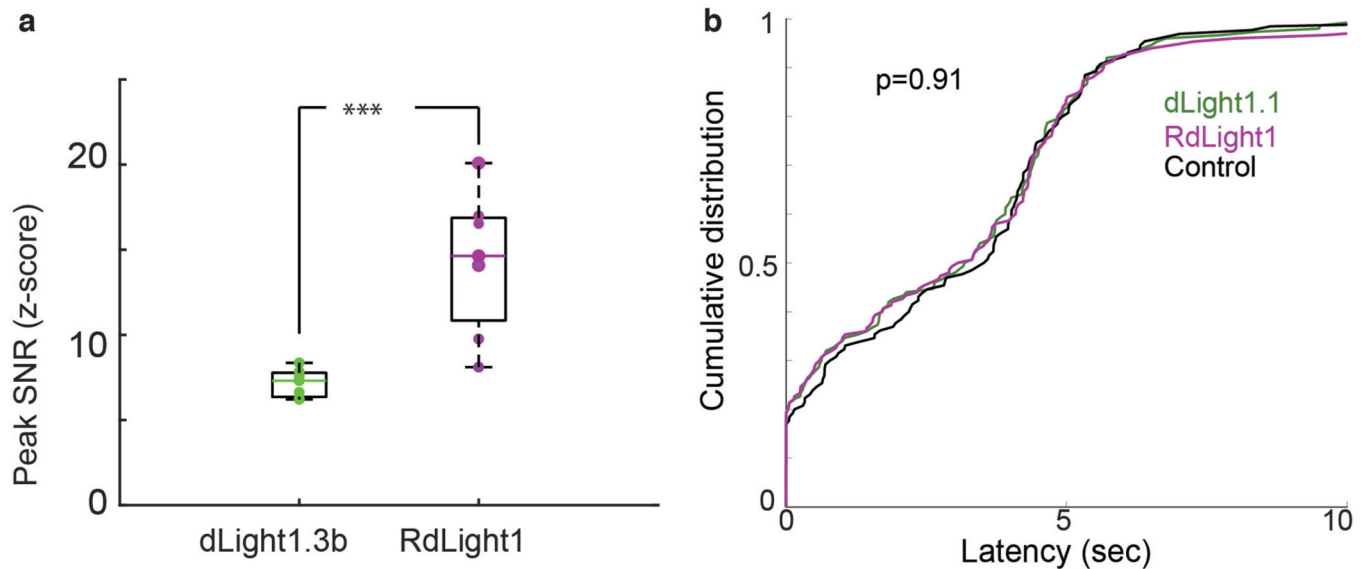
Extended Data Fig. 10. In vivo signal-to-noise ratio comparison between RdLight1 and dLight1.3b, and effect of dLight1.1 or RdLight1 expression in NAc on motivated approach behavior.

a, Peak response to an unpredicted click signaling immediate reward delivery. Signals were collected using fiber photometry

across n=6 rats with dLight1.3b expressed in NAc and n=7 rats with RdLight1 expressed in the same coordinates. RdLight1 signals demonstrated significantly higher signal-to-noise ratio (SNR). A one-sided t-test was used to assess statistical significance (p=8.04×10^−3). Box plot shows the mean and quartiles of the data with whiskers representing the range of observations. **b**, To investigate the effect of dopamine indicators on behavior, we compared two cohorts of rats expressing either dLight1.1 (n=8) or RdLight1 (n=6) in NAc to a control group (n=6) expressing neither. Similar to the experimental paradigm for the in vivo photometry experiments, rats are placed in an operant chamber with a speaker and a reward delivery port. An auditory click indicating an immediate delivery of a sucrose pellet is played at random intervals. Rats with either of the indicators expressed in NAc show no difference to the control group in their latency to approach and retrieve the reward following the click. A kolmogorov-smirnov test was used to compare the latency distributions.

Supplementary Material

Refer to Web version on PubMed Central for supplementary material.

ACKNOWLEDGEMENTS

References

1. Patriarchi T. et al. Ultrafast neuronal imaging of dopamine dynamics with designed genetically encoded sensors. Science 360, eaat4422 (2018).

2. Sun F. et al. A Genetically Encoded Fluorescent Sensor Enables Rapid and Specific Detection of Dopamine in Flies, Fish, and Mice. Cell 174, 481–496.e19 (2018). [PubMed: 30007419]

3. de Jong JW et al. A Neural Circuit Mechanism for Encoding Aversive Stimuli in the Mesolimbic Dopamine System. Neuron 101, 133–151.e7 (2019). [PubMed: 30503173]

4. Mohebi A. et al. Dissociable dopamine dynamics for learning and motivation. Nature 570, 65–70 (2019). [PubMed: 31118513]

5. Zhao Y. et al. An Expanded Palette of Genetically Encoded Ca2+ Indicators. Science 333, 1888–1891 (2011). [PubMed: 21903779]

6. Dana H. et al. Sensitive red protein calcium indicators for imaging neural activity. eLife 5, e12727 (2016). [PubMed: 27011354]

7. Kruss S. et al. High-resolution imaging of cellular dopamine efflux using a fluorescent nanosensor array. PNAS 114, 1789–1794 (2017). [PubMed: 28179565]

8. Beyene AG et al. Imaging striatal dopamine release using a nongenetically encoded near infrared fluorescent catecholamine nanosensor. Science Advances 5, eaaw3108 (2019).

9. Wachter RM, Elsliger MA, Kallio K, Hanson GT & Remington SJ Structural basis of spectral shifts in the yellow-emission variants of green fluorescent protein. Structure 6, 1267–1277 (1998). [PubMed: 9782051]

10. Orm M. et al. Crystal Structure of the Aequorea victoria Green Fluorescent Protein. Science 273, 1392–1395 (1996). [PubMed: 8703075]

11. Nagai T. et al. A variant of yellow fluorescent protein with fast and efficient maturation for cell-biological applications. Nat. Biotechnol. 20, 87–90 (2002). [PubMed: 11753368]

12. Ade K, Wan Y, Chen M, Gloss B. & Calakos N. An Improved BAC Transgenic Fluorescent Reporter Line for Sensitive and Specific Identification of Striatonigral Medium Spiny Neurons. Front. Syst. Neurosci. 5, (2011).

13. Eichel K. et al. Catalytic activation of β-arrestin by GPCRs. Nature 557, 381–386 (2018). [PubMed: 29720660]

14. Kebabian JW et al. A-77636: a potent and selective dopamine D1 receptor agonist with antiparkinsonian activity in marmosets. Eur. J. Pharmacol. 229, 203–209 (1992). [PubMed: 1362704]

15. Oe Y. et al. Distinct temporal integration of noradrenaline signaling by astrocytic second messengers during vigilance. Nat Commun 11, 471 (2020). [PubMed: 31980655]

16. Marvin JS et al. An optimized fluorescent probe for visualizing glutamate neurotransmission. Nat Methods 10, 162–170 (2013). [PubMed: 23314171]

17. Villette V. et al. Ultrafast Two-Photon Imaging of a High-Gain Voltage Indicator in Awake Behaving Mice. Cell 179, 1590–1608.e23 (2019). [PubMed: 31835034]

18. Chen T-W et al. Ultrasensitive fluorescent proteins for imaging neuronal activity. Nature 499, 295–300 (2013). [PubMed: 23868258]

19. Witten IB et al. Recombinase-driver rat lines: tools, techniques, and optogenetic application to dopamine-mediated reinforcement. Neuron 72, 721–733 (2011). [PubMed: 22153370]

20. Hamid AA et al. Mesolimbic Dopamine Signals the Value of Work. Nat Neurosci 19, 117–126 (2016). [PubMed: 26595651]

21. Stujenske JM, Spellman T. & Gordon JA Modeling the Spatiotemporal Dynamics of Light and Heat Propagation for In Vivo Optogenetics. Cell Rep 12, 525–534 (2015). [PubMed: 26166563]

22. Broussard GJ et al. In vivo measurement of afferent activity with axon-specific calcium imaging. Nat Neurosci 21, 1272–1280 (2018). [PubMed: 30127424]

23. Pettibone JR et al. Knock-In Rat Lines with Cre Recombinase at the Dopamine D1 and Adenosine 2a Receptor Loci. eNeuro 6, (2019).

24. Hnasko TS et al. Vesicular glutamate transport promotes dopamine storage and glutamate corelease in vivo. Neuron 65, 643–656 (2010). [PubMed: 20223200]

25. Schultz W. Dopamine reward prediction-error signalling: a two-component response. Nature Reviews Neuroscience 17, 183–195 (2016). [PubMed: 26865020]

26. Kalivas PW & Duffy P. Dopamine regulation of extracellular glutamate in the nucleus accumbens. Brain Research 761, 173–177 (1997). [PubMed: 9247082]

27. Marvin JS et al. Stability, affinity, and chromatic variants of the glutamate sensor iGluSnFR. Nature Methods 15, 936–939 (2018). [PubMed: 30377363]

28. Dana H. et al. High-performance calcium sensors for imaging activity in neuronal populations and microcompartments. Nat Methods 16, 649–657 (2019). [PubMed: 31209382]

29. Gerfen CR & Surmeier DJ Modulation of Striatal Projection Systems by Dopamine. Annual Review of Neuroscience 34, 441–466 (2011).

30. Planert H, Berger TK & Silberberg G. Membrane Properties of Striatal Direct and Indirect Pathway Neurons in Mouse and Rat Slices and Their Modulation by Dopamine. PLOS ONE 8, e57054 (2013). [PubMed: 23469183]

31. Ishikawa A, Ambroggi F, Nicola SM & Fields HL Dorsomedial Prefrontal Cortex Contribution to Behavioral and Nucleus Accumbens Neuronal Responses to Incentive Cues. J. Neurosci. 28, 5088–5098 (2008). [PubMed: 18463262]

32. Burgos-Robles A, Bravo-Rivera H. & Quirk GJ Prelimbic and Infralimbic Neurons Signal Distinct Aspects of Appetitive Instrumental Behavior. PLOS ONE 8, e57575 (2013). [PubMed: 23460877]

33. Ambroggi F, Ishikawa A, Fields HL & Nicola SM Basolateral amygdala neurons facilitate reward-seeking behavior by exciting nucleus accumbens neurons. Neuron 59, 648–661 (2008). [PubMed: 18760700]

34. Bamford NS, Wightman RM & Sulzer D. Dopamine's Effects on Corticostriatal Synapses during Reward-Based Behaviors. Neuron 97, 494–510 (2018). [PubMed: 29420932]

35. Rice ME & Cragg SJ Dopamine spillover after quantal release: Rethinking dopamine transmission in the nigrostriatal pathway. Brain Research Reviews 58, 303–313 (2008). [PubMed: 18433875]

36. Hnasko TS, Hjelmstad GO, Fields HL & Edwards RH Ventral Tegmental Area Glutamate Neurons: Electrophysiological Properties and Projections. J. Neurosci. 32, 15076–15085 (2012). [PubMed: 23100428]

37. McFarland K. & Kalivas PW The Circuitry Mediating Cocaine-Induced Reinstatement of Drug-Seeking Behavior. J. Neurosci. 21, 8655–8663 (2001). [PubMed: 11606653]

38. Hioki H. et al. Efficient gene transduction of neurons by lentivirus with enhanced neuron-specific promoters. Gene Therapy 14, 872–882 (2007). [PubMed: 17361216]

39. Nicola SM, Taha SA, Kim SW & Fields HL Nucleus accumbens dopamine release is necessary and sufficient to promote the behavioral response to reward-predictive cues. NEUROSCIENCE 135, 1025–1033 (2005). [PubMed: 16165291]

40. Feng J. et al. A Genetically Encoded Fluorescent Sensor for Rapid and Specific In Vivo Detection of Norepinephrine. Neuron 102, 745–761.e8 (2019). [PubMed: 30922875]

41. Jing M. et al. A genetically encoded fluorescent acetylcholine indicator for in vitro and in vivo studies. Nat Biotechnol 36, 726–737 (2018). [PubMed: 29985477]

42. Qian Y. et al. A genetically encoded near-infrared fluorescent calcium ion indicator. Nat Methods 16, 171–174 (2019). [PubMed: 30664778]

43. Ravotto L, Duffet L, Zhou X, Weber B. & Patriarchi T. A Bright and Colorful Future for G-Protein Coupled Receptor Sensors. Front. Cell. Neurosci. 14, (2020).

Methods-only References

43. Quan J. & Tian J. Circular polymerase extension cloning. Methods Mol. Biol. 1116, 103–117 (2014). [PubMed: 24395360]

44. Tian L. et al. Imaging neural activity in worms, flies and mice with improved GCaMP calcium indicators. Nat Methods 6, 875–881 (2009). [PubMed: 19898485]

45. Song Y. et al. High-Resolution Comparative Modeling with RosettaCM. Structure 21, 1735–1742 (2013). [PubMed: 24035711]

46. Rasmussen SGF et al. Structure of a nanobody-stabilized active state of the β2 adrenoceptor. Nature 469, 175–180 (2011). [PubMed: 21228869]

47. Chen Y. et al. Structural insight into enhanced calcium indicator GCaMP3 and GCaMPJ to promote further improvement. Protein Cell 4, 299–309 (2013). [PubMed: 23549615]

48. Bender BJ et al. Protocols for Molecular Modeling with Rosetta3 and RosettaScripts. Biochemistry 55, 4748–4763 (2016). [PubMed: 27490953]

49. Kotowski SJ, Hopf FW, Seif T, Bonci A. & von Zastrow M. Endocytosis Promotes Rapid Dopaminergic Signaling. Neuron 71, 278–290 (2011). [PubMed: 21791287]

50. Patriarchi T. et al. Imaging neuromodulators with high spatiotemporal resolution using genetically encoded indicators. Nature Protocols 14, 3471–3505 (2019). [PubMed: 31732722]

51. Irannejad R. et al. Conformational biosensors reveal GPCR signalling from endosomes. Nature 495, 534–538 (2013). [PubMed: 23515162]

52. Tewson PH, Martinka S, Shaner NC, Hughes TE & Quinn AM New DAG and cAMP Sensors Optimized for Live-Cell Assays in Automated Laboratories. J Biomol Screen 21, 298–305 (2016). [PubMed: 26657040]

53. Ke M-T, Fujimoto S. & Imai T. SeeDB: a simple and morphology-preserving optical clearing agent for neuronal circuit reconstruction. Nat Neurosci 16, 1154–1161 (2013). [PubMed: 23792946]
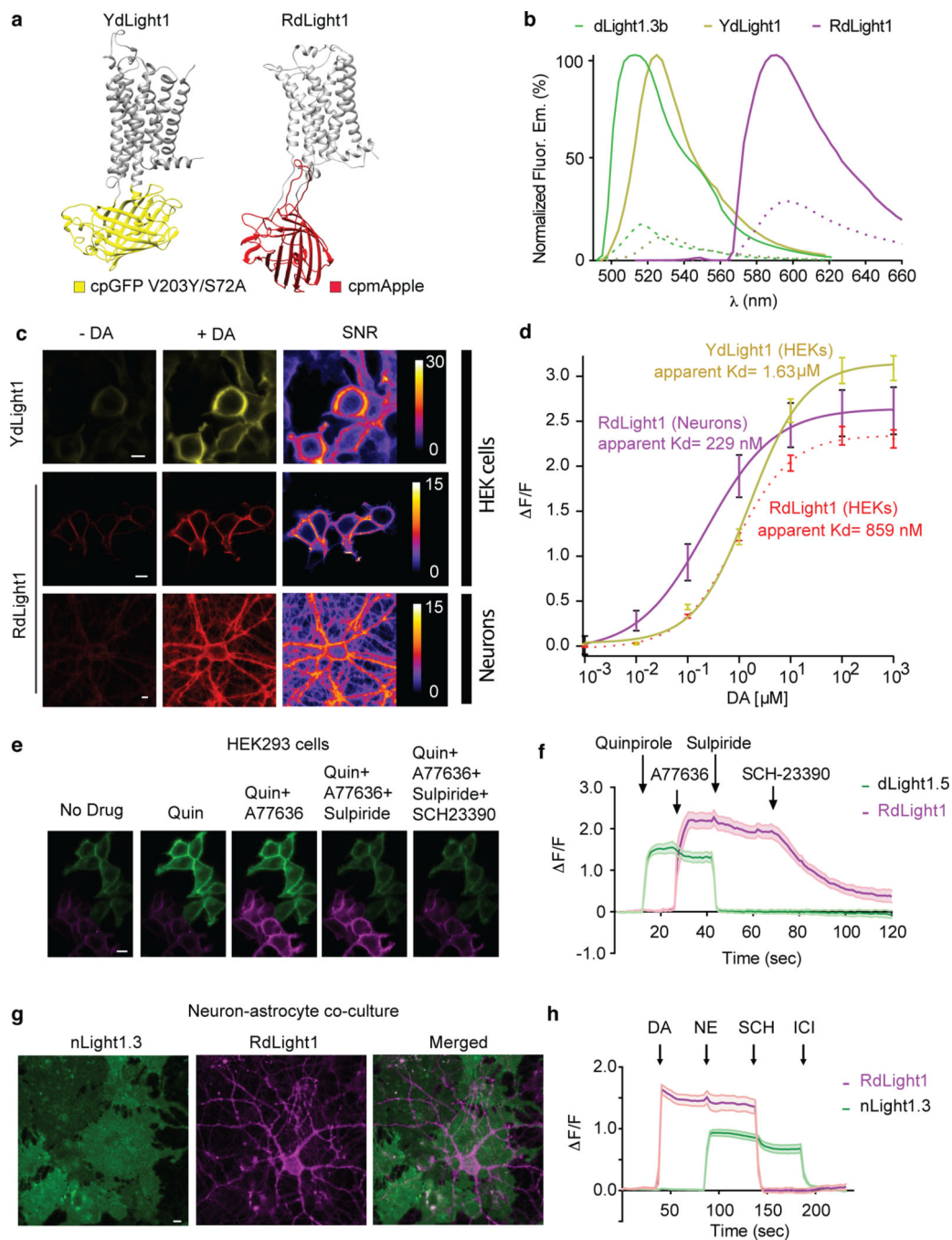
Figure 1 |. Engineering and characterization of red-shifted dLight1 variants.
a, simulated structure of yellow and red dopamine sensors. **b**, Emission spectra of dLight1.3b, YdLight1 and RdLight1. The fluorescence emission was measured in HEK293 cells before (dotted lines) and after (continuous lines) addition of 100 μM DA to the medium. **c,**In vitro characterization of dLight1.3b spectral variants. Representative images showing expression and fluorescence response of YdLight1 and of RdLight1 in HEK293 cells and dissociated hippocampal neurons. SNR heatmaps were calculated based on the response to 100 μM DA. n = 3 cells from 3 separate experiments. Scale bars, 10 μm. **d**, In

situ titration of DA on HEK293 cells. Apparent affinity values (apparent K_d) are defined as the concentration of the ligand producing 50% of maximal fluorescence changes (max F/F). YdLight1: apparent K_d= 1.63 ± 0.26 μM (n=9 cells); RdLight1: apparent K_d= 859 ± 7 nM (n=26 cells) in HEK293 cells and 229 ± 2 nM (n=15 cells) in neurons. mean ± SEM. **e**, Multiplex imaging of drug efficacy at distinct dopamine receptor subtypes. Left, representative images of HEK293 cells expressing either dLight1.5 or RdLight1 and their average fluorescent responses to individual drugs. Scale bars, 10 μm. **f**, Fluorescence responses of both sensors in (**e**) during drug application are shown. Maximal fluorescent responses: green channel after quinpirole (10 μM) (F/F = 155 ± 14%), red channel after A77636 (100 nM) (F/F = 221 ± 19%), green channel after sulpride (400 nM)(F/F =1 ± 3%), red channel after SCH-23390(10 μM) (F/F = 32 ± 17%). n = 6 cells from 3 cultures. mean ± SEM. **g**, Multiplexed imaging in neuron-astrocyte co-culture. Cells were transduced with AAV1.*GFAP*.nLight1.3 and AAV.*hSynapsin1*.RdLight1 14 days prior to imaging, for selective expression of nLight1.3 in astrocytes and RdLight1 in neurons. Representative images of sensor-expressing cells are shown. n = 3 cells from 3 separate experiments. Scale bar, 10 μm. **h**, Fluorescence responses in (**g**) to bath-applied DA, NE, SCH-23390 (SCH), ICI118551 (ICI), all drugs were used at 1 μM. n = 3 cells from 3 separate experiments. mean ± SEM.
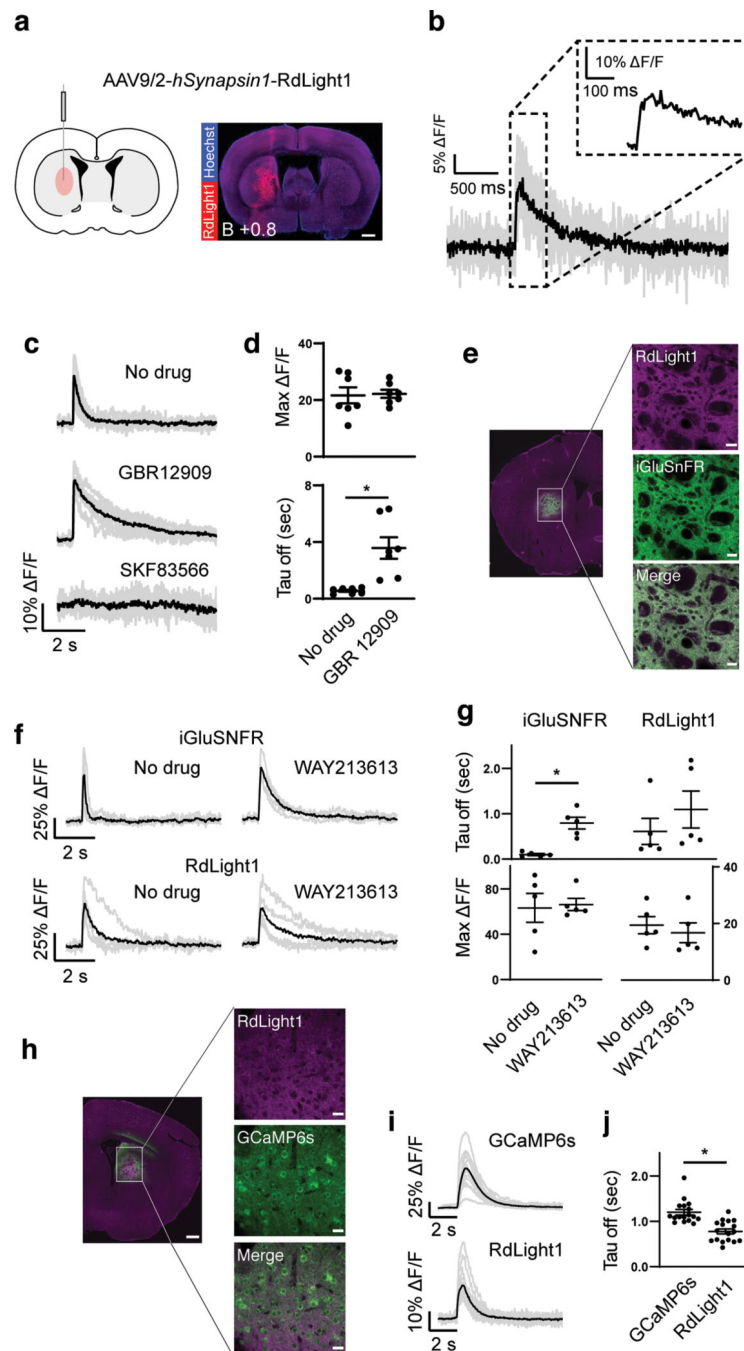
Figure 2 |. Two-photon imaging of RdLight1 in acute brain slices.
a, Schematic representation of viral injection in dorsal striatum of mice (left panel), and representative image of RdLight1 expression in the striatum from a SeeDB [53] cleared brain slice (right panel, n=2 mice). Scale bar, 1 mm. **b**, Single-trial fluorescence responses (average in black) of RdLight1 in response to a single stimulus (4 V, 0.5ms) acquired at 198 Hz. Averaged fluorescence fold-change (ΔF/F) = $20.2 \pm 1.8\%$ across 7 trials from 3 mice, $Tau_{on} = 14.1 \pm 1.5$ ms and $Tau_{off} = 0.398 \pm 0.058$ s, mean $\pm$ SEM. Inset shows zoomed-in view of the fluorescence peak. **c**, Single-trial fluorescence responses (average in black) of

RdLight1 in response to a single stimulus (4 V, 0.5 ms) in the presence of GBR12909 (1 μM, Tau off = 3.580 ± 0.764 s), or SKF83566 (10 μM) acquired at 30 Hz. n = 7 trials from 4 mice. **d**, Quantification of maximal fluorescence fold-change (F/F) and decay time in (**c**). Peak fluorescence: no drug, 21.7 ± 2.8%; GBR12909, 22.2 ± 2.0%; p = 0.800, paired t-test (two-sided). Decay time: no drug, 0.560 ± 0.076 s; GBR12909, 3.580 ± 0.764 s; *p = 0.009, paired t-test (two-sided). n = 7 trials from 4 mice, mean ± SEM. **e**, Representative histology images of iGluSNFR and RdLight1 expression (n=2 mice). Scale bar, 0.5 mm or 20 μm. **f**, Single-trial fluorescence responses (average in black from 5 trials of 3 mice) of simultaneously recorded iGluSNFR and RdLight1 in response to electrical stimulation (5 pulses, 4 V, 0.2ms at 40 Hz) before and during application of WAY213613 (20 μM). RdLight1, F/F = 19.4 ± 3.0 %, Tau off = 0.611 ± 0.288 sec; iGluSNFR, F/F_{max} = 63.3 ± 12.8 %, Tau off = 0.100 ± 0.024 sec; Images acquired at 30 Hz. **g**, Quantification of decay time and maximal fluorescence fold-change (F/F) for the responses in (**f**). For iGluSNFR, decay time in no drug: 0.100 ± 0.024 s, with WAY213613: 0.792 ± 0.129 s, *p = 0.005, paired t-test (two-sided); peak fluorescence in no drug: 63.3 ± 12.8%, with WAY213613: 66.3 ± 5.4%, p = 0.798, paired t-test (two-sided). For RdLight1, decay time in no drug: 0.611 ± 0.288 s, with WAY213613: 1.093 ± 0.409 s, p = 0.123, paired t-test (two-sided); peak fluorescence in no drug: 19.4 ± 3.0%, with WAY213613: 16.7 ± 3.5%, p = 0.093, paired t-test (two-sided). n = 5 trials from 3 mice, mean ± SEM. **h**, Representative histology images of RdLight1 and GCaMP6s expression (n=2 mice). Scale bar, 0.5 mm or 20 μm. **i**, Representative single-trial fluorescence responses (average in black from 17 trials of 10 mice) of simultaneously recorded GCaMP6s and RdLight1 in response to electrical stimulation (20 pulses, 4 V, 0.2 ms at 40 Hz). Images acquired at 30 Hz **j**, Quantification of decay time response in (**i**). GCaMP6s: 1.202 ± 0.061 s; RdLight1: 0.778 ± 0.055 s. *p = 0.0002, paired t-test (two-sided). n = 17 trials from 10 mice, mean ± SEM.
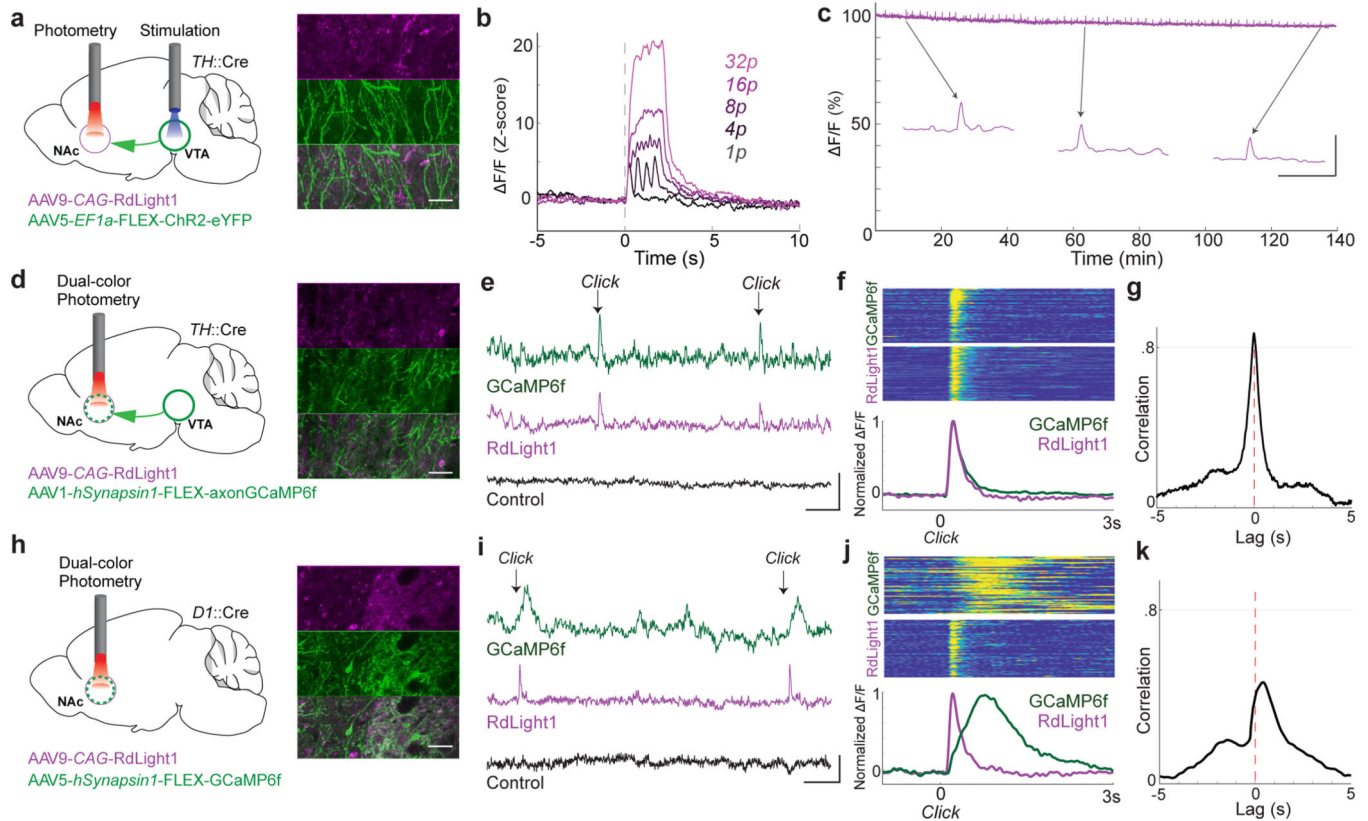
Figure 3 |. Combining RdLight1 with optogenetics and calcium monitoring *in vivo*.
a, Left: Schematic representation of viral injections and fiber implants in NAc and VTA, using TH-Cre rats and Cre-dependent virus to drive ChR2 expression selectively in dopamine neurons. Right: representative micrograph showing RdLight1 in magenta and ChR2-eYFP in green (n=2 rats). Scale bar, 50 μm. **b,** Mean fluorescence changes of RdLight1 across all trials (n=250 trials) in NAc produced by blue light (462 nm, 10 mW at fiber tip) stimulation of VTA. Light pulses were 2 ms in duration, and given as either a single pulse (1p) or a two second duration train with the indicated number of pulses. **c,** Single-trial fluorescence changes of RdLight1 over prolonged monitoring *in vivo*. The rat was given 60 rewards at unpredictable times over a >2 hr period. Individual reward responses shown in insets. At 2 hrs, fluorescence = 95.3% +− 0.034 (mean +− SEM) of starting fluorescence(n=4 rats); Inset scale bars: 5ms, 5% F/F. **d,** Left: Schematic of dual-color photometry, again in TH-Cre rats but this time using virus to drive axon-targeted GCaMP6f in dopamine terminals. Right: representative micrograph showing RdLight1 in magenta and axon-GCaMP6f in green(n=2 rats). Scale bar, 50 μm. **e,** Single-trial fluorescence (n=60 trials)changes from simultaneous recording of RdLight1 555–570 nm/ 580–680 nm (excitation/emission), GCaMP6f 460–490 nm/500–540 nm(excitation/ emission), and isosbestic (non-calcium-dependent 400–410 nm/500–540 nm (excitation/ emission) control around unexpected, audible reward deliveries ("Clicks" of the food hopper). Scale bars: 6s, 5% F/F. **f,** Top, fluorescence changes of all trials (n=60 trials) of unexpected reward deliveries. Yellow = maximum. Bottom, mean fluorescence changes across all trials (n=120 trials from two rats). RdLight1 tau_{on} = 126 ± 15 ms and tau_{off} = 320

± 42 ms, mean ± SEM. Tau_{on} was calculated by fitting this average RdLight1 fluorescence rise with linear regression and tau_{off} was calculated by fitting the fluorescence decay with a single exponential curve. **g,** Session-wide cross-correlation between presynaptic calcium in dopamine terminals, and dopamine release. Peak correlation = 0.86 ± 0.06 at zero lag (n=2 sessions). **h-k**, as **c-f**, but with GCaMP6f expressed in D1+ cells (in D1-Cre rats). Session-wide cross-correlation (average of two rats) between RdLight1 and GCaMP6f, peak = 0.54 at lag of 372 ms (dopamine leading). Scale bar, 50 μm.
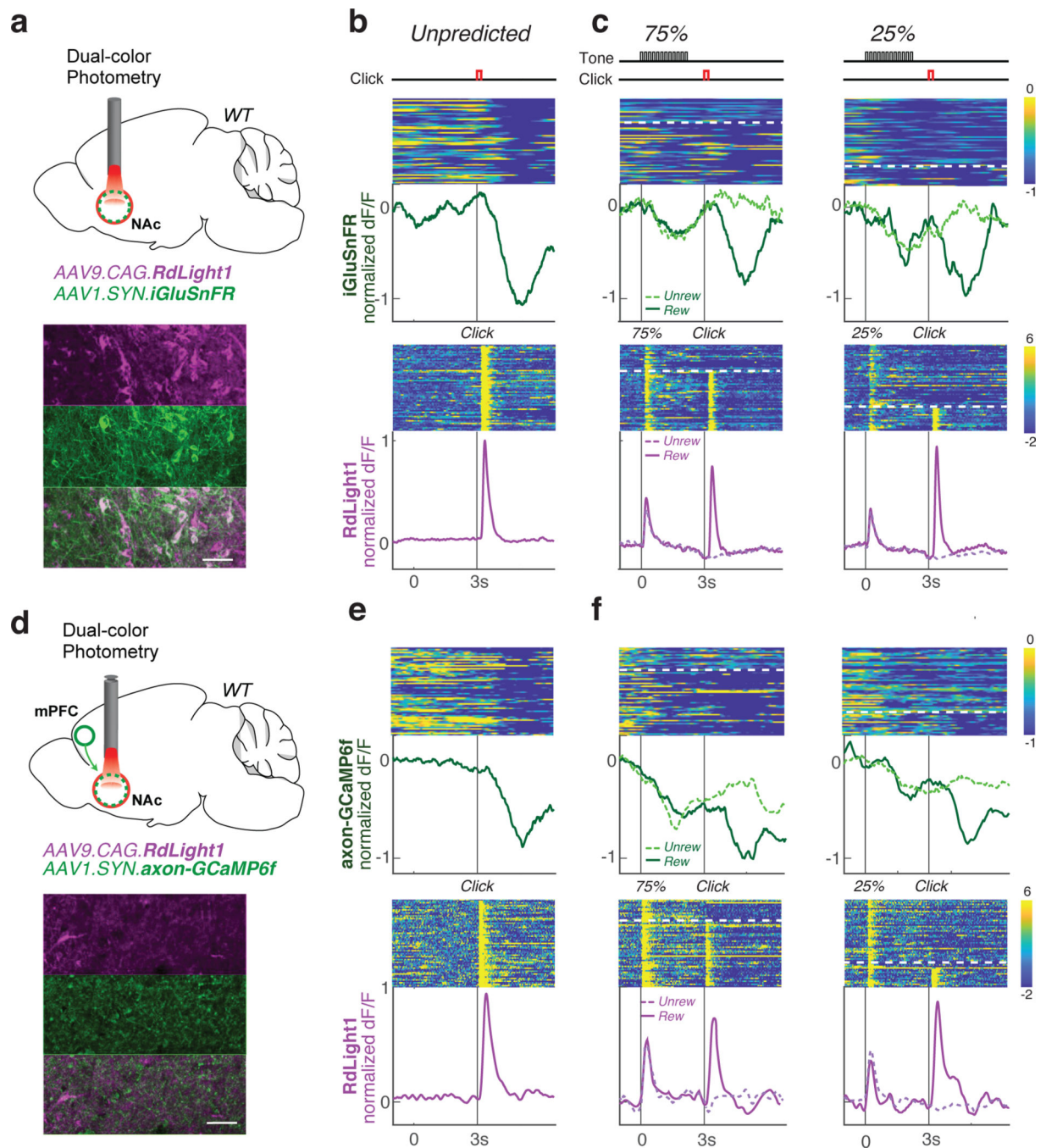
Figure 4 |. Combining RdLight1 with glutamate monitoring *in vivo*.
a, Top: Schematic representation of dual-color photometry in NAc, using wild type rats co-expressing RdLight1 and iGluSnFR injected in NAc. Bottom: example micrograph showing RdLight1 in magenta and iGluSnFR in green (n=2 rats). Scale bar, 50 μm. **b,** iGluSnFR and RdLight1 signal changes in NAc following unpredicted reward delivery. Top, fluorescence changes of all trials to unexpected reward deliveries (n=60 trials). Bottom, mean fluorescence changes across all trials (n=120 trials from two rats). **c,** Tones (of different frequencies) signaled availabilities of reward deliveries with different probabilities (75% or

25%) after a fixed period of 3s. Solid and dotted lines indicate rewarded and unrewarded trials respectively for iGluSnFR in green and RdLight1 in magenta. Top, fluorescence changes of all trials to unexpected reward deliveries (n=60 trials). Bottom, mean fluorescence changes across all trials (n=120 trials from two rats). **d,** Top**:** Schematic of dual-color photometry in NAc, using wild type rats co-expressing RdLight1 injected in NAc and axon-GCaMP6f injected in mPFC. Bottom: representative micrograph showing RdLight1 in magenta and axon-GCaMP6f in green (n=2 rats). Scale bar, 50 μm. **e-f,** Same as **b-c** except for axon-GCaMP6f measurement instead of iGluSnFR.